APPLICATION OF AN OPTIMAL CONTROL PILOT MODEL TO AIR-TO-AIR COMBAT

Thomas R. Harvey

Air Force Institute of Technology
Wright-Patterson Air Force Base, Ohio

March 1974

APPLICATION OF AN OPTIMAL CONTROL PILOT MODEL TO AIR-TO-AIR COMBAT

THESIS

GA/MA/74M-1 Thomas R. Harvey
Captain USAF

Approved for public release; distribution unlimited.

GA/MA/74M-1

APPLICATION OF AN OPTIMAL CONTROL PILOT MODEL TO AIR-TO-AIR COMBAT

THESIS

Presented to the Faculty of the School of Engineering

of the Air Force Institute of Technology

Air University

in Partial Fulfillment of the

Requirements for the Degree of

Master of Science

by

Thomas R. Harvey, B.S.E.E.

Captain USAF

Graduate Astronautical Engineering

March 1974

Approved for public release; distribution unlimited.

jc

Preface

We live in a very complex world. Time was when a man could be a jack-of-all-trades and master them all. Not so anymore. Today a jack-of-all-trades would be master of none. Becoming a master of just one trade now requires near total committment to it not just in the apprenticeship stages, but also in the years that follow merely to keep abreast of the constant changes.

Having been a full-time U. S. Air Force pilot for the six years prior to arriving at the Air Force Institute of Technology, I found out the truth of that statement very quickly. I earned my B. S. degree in electrical engineering six years before, but by this time neglect of all things mathematical had taken its toll on any engineering skill I may once have possessed. So, my 19-month tenure at AFIT was a long, hard struggle to re-establish myself in the engineering world.

It is for this reason that I am truly grateful to my thesis advisor, Major James D. Dillow, for his constant encouragement and help on the work presented herein. I would also like to thank Mr. Ronald O. Anderson of the Flight Simulation Branch, Air Force Flight Dynamics Laboratory, for his support on this project. A special thanks, also, to Mr. Allan Carney for his eager assistance in setting up the analog simulation. Upon his aid much of the success of the simulation rests.

Of course, this work would never have gotten off the ground without the cooperation of my three pilots. I am deeply indebted to Captains Jim Butt, Ed Jordan, and Jim Tilley for foregoing what precious little free time students at AFIT enjoy and spending many hours apiece flying my simulation.

And, finally, for putting up with a non-existent husband for these past 19 months, a special debt of gratitude is extended to my wife, Trish. She bravely carried on through thick and thin.

Thomas R. Harvey

UNCLASSIFIED

SECURITY CLASSIFICATION OF THIS PAGE (When Data Entered)

AD 777847

REPORT DOCUMENTATION PAGE

READ INSTRUCTIONS BEFORE COMPLETING FORM

1. REPORT NUMBER: GA/MA/74M-1	2. GOVT ACCESSION NO.
3. RECIPIENT'S CATALOG NUMBER	
4. TITLE (and Subtitle): APPLICATION OF AN OPTIMAL CONTROL PILOT MODEL TO AIR-TO-AIR COMBAT	5. TYPE OF REPORT & PERIOD COVERED: MS Thesis
	6. PERFORMING ORG. REPORT NUMBER
7. AUTHOR(s): Thomas R. Harvey, Captain, USAF	8. CONTRACT OR GRANT NUMBER(s)
9. PERFORMING ORGANIZATION NAME AND ADDRESS: Air Force Institute of Technology (AFIT-EN), Wright-Patterson AFB, Ohio 45433	10. PROGRAM ELEMENT, PROJECT, TASK AREA & WORK UNIT NUMBERS: 62201F/1986-02-02
11. CONTROLLING OFFICE NAME AND ADDRESS: Systems Dynamics Branch/Flight Control Division, Air Force Flight Dynamics Laboratory, Wright-Patterson AFB, Ohio 45433	12. REPORT DATE: March, 1974
	13. NUMBER OF PAGES: 102
14. MONITORING AGENCY NAME & ADDRESS (if different from Controlling Office)	15. SECURITY CLASS. (of this report): Unclassified
	15a. DECLASSIFICATION DOWNGRADING SCHEDULE

16. DISTRIBUTION STATEMENT (of this Report)

Approved for public release; distribution unlimited

17. DISTRIBUTION STATEMENT (of the abstract entered in Block 20, if different from Report)

18. SUPPLEMENTARY NOTES

Approved for public release; IAW AFR 190-17

JERRY C. HIX, Captain, USAF
Director of Information

19. KEY WORDS (Continue on reverse side if necessary and identify by block number)

Air-to-Air Combat
Optimal Control
Pilot Modeling
Analog Computer Simulation
Kalman Filter Application

20. ABSTRACT (Continue on reverse side if necessary and identify by block number)

The two-dimensional (longitudinal) kinematics of air-to-air combat tracking with a lead computing optical sight system were simulated on an analog computer. Three pilots flew three different aircraft configurations on the fixed-base simulator at 3000- and 1000-foot ranges against a target driven to RMS accelerations of 3.5 G and 5.0 G by filtered, white, Gaussian noise. Averaged RMS data were recorded on attacker's elevator deflection, pitch rate, lead angle, line of sight to the target, and tracking error for each case.

(CONTINUED ON REVERSE SIDE)

DD FORM 1 JAN 73 1473 EDITION OF 1 NOV 65 IS OBSOLETE

UNCLASSIFIED

SECURITY CLASSIFICATION OF THIS PAGE (When Data Entered)

Block 20, Abstract (Continued)

Simultaneously, the identical tasks were performed by a digital pilot model formulated from optimal control theory with visual acuity threshold affects accounted for. A comparison of the data generated by the human pilots versus that of the pilot model showed very nearly a one-to-one correlation for elevator deflection, lead angle, and line of sight. However, the results were not quite as comparable when applied to pitch rate and tracking error. A re-evaluation of cost functional weightings based upon a further analysis of pilot response in this task led to model performance that correlated with the human pilot performance data very well.

Contents

List of Figures

Figure | Page

List of Tables

Notation

Note: Underlined variables in this report indicate column vectors. Capital letters in vector equations are matrices.

A	System plant matrix
A_{n_A}	Attacker acceleration normal to longitudinal axis
A_{n_T}	Target acceleration normal to longitudinal axis
$\underline{b}$	System control vector
C	Error Covariance matrix
C_{L_α}	Rate of change of lift coefficient with angle of attack (dimensionless)
C_{L_δ}	Rate of change of lift coefficient with elevator deflection (dimensionless)
D	Present range
$E\{\cdot\}$	Expected value operator
F_s	Force applied to control stick
$f(y)$	Visual threshold gain factor
G	Kinematic acceleration forces (1 G = 32.2 ft/sec^2)
g	Control rate weighting
H	System observation matrix
$J(\cdot)$	Cost functional
J_v	Ballistic jump parameter
K_B	Ballistic parameter
K_f	Force stick sensitivity
K_L	Control linkeage gain
K_o	Riccati gains
M_α, $M_{\dot{\alpha}}$	Aircraft stability derivatives relating pitching moment to angle of attack and angle of attack rate
M_δ	Aircraft stability derivative relating pitching moment to elevator deflection

M_q	Aircraft stability derivatives relating pitching moment to pitch rate
Q	State weighting matrix
Q'	Weighting matrix for observed variables
q_{ij}	Element of Q
q	Pitch rate of attacker
r	Control weighting
R_p	Range of projectile from attacker firing position
R_T	Range of target from attacker firing position
$\underline{s}$	Unit vector along line of sight
s	Laplace operator
t	Time
T	Tracking time in simulation
T_f	Projectile time of flight
u	Pilot control input to system
u_c	Commanded control input
V_A	Attacker velocity
V_f	Mean relative velocity of the projectile over one time of flight
V_I	Total projectile velocity at muzzle
V_m	Projectile muzzle velocity
V_p	Projectile velocity
V_T	Target velocity
V_u	Covariance of motor noise
V_y	Covariance of observation noise
V_{avg}	Average inertial projectile velocity
v_u	Motor noise
v_y	Observation noise

W	Covariance of noise input to system dynamics
w	Noise input to system dynamics
WL	Weapon line
x	State variable
y	Observation variable
y_p	Noise-corrupted observed variable
$\underline{z}$	Augmented system state vector
Z	Covariance of $\underline{z}$
Z_α	Aircraft dimensional stability derivative relating normal force to angle of attack
Z_δ	Aircraft dimensional stability derivatives relating normal force to elevator deflection
α	Angle of attack of attacker
γ_A	Flight path angle of attacker
γ_T	Flight path angle of target
δ	Elevator deflection angle of attacker
$\delta(t - \tau)$	Kronecker delta function
δ_c	Commanded elevator deflection angle
ε	Tracking error angle
ζ	Dummy state used in predictor
η	Dummy variable, $= CH_1^T V_y^{-1} + \underline{b}_1 e^{-s\tau}$
θ	Pitch angle of attacker
ℓ	Optimal feedback gains
λ	Lead angle
μ	Noise-corrupted commanded control input
ξ	White noise
ρ	Atmospheric density
ρ_o	Sea level atmospheric density
ρ_i, ρ_u	Constants for computation of noise covariance

Σ_p	Inertial angular position of sight reticle
Σ_T	Inertial line of sight (LOS) angle from attacker to target
Σ_{T_A}	Relative line of sight angle from attacker to target
σ	Dummy variable of integration
σ_x	RMS value of x
τ	Pilot time lag
τ_a	Time constant of actuator
τ_N	Pilot neuro-muscular time constant
τ_T	Target time constant

Abstract

The two-dimensional (longitudinal) kinematics of air-to-air combat tracking with a lead computing optical sight system were simulated on an analog computer. Three pilots flew three different aircraft configurations on the fixed-base simulator at 3000- and 1000-foot ranges against a target driven to RMS accelerations of 3.5 G and 5.0 G by filtered, white, Gaussian noise. Averaged RMS data were recorded on attacker's elevator deflection, pitch rate, lead angle, line of sight to the target, and tracking error for each case.

Simultaneously, the identical tasks were performed by a digital pilot model formulated from optimal control theory with visual acuity threshold effects accounted for. A comparison of the data generated by the human pilots versus that of the pilot model showed very nearly a one-to-one correlation for elevator deflection, lead angle, and line of sight. However, the results were not quite as comparable when applied to pitch rate and tracking error. A re-evaluation of cost functional weightings based upon a further analysis of pilot response in this task led to model performance that correlated with the human pilot performance data very well.

APPLICATION OF AN OPTIMAL CONTROL PILOT MODEL TO AIR-TO-AIR COMBAT

I. Introduction

A Problem Exists

All too often production engineering runs into design problems at the final stages of production due to incompatibility of integrated subsystems. This problem is especially critical when the system is being designed for use by a human operator. The reason for this anomaly is the fact that, even though individual subsystems may be designed perfectly for the task that is to be performed, when they are integrated by means of a human operator, the overall system can break down because of the operator's inherent complexities and imperfections. For example, if a subsystem is designed with very little stability margin, the lag time inherent in the human operator's reaction might well cause the system to become unstable. This is due to the fact that the action of the operator could actually degrade the combined action rather than achieve the stabilizing effect intended. Therefore, increased emphasis is being placed on total system simulation with the pilot in the loop during the preliminary design stages of production.

These system simulations usually take one of two forms. The first is direct simulation of the total system on analog or hybrid computers. This demands a human operator to close the control loop by performing the design task. The second method involves mathematical simulation of the

operator. This model is used to predict human operator reaction to system design and to evaluate the compatibility of the integrated system. The latter method alleviates the need for the repetitive data collection process required when the human operator is used in the simulation, so long as it can be shown that the mathematical pilot model successfully duplicates human pilot reaction. The objective of this analysis is to show that a mathematical pilot model can accurately predict the performance of integrated aircraft flight control and lead computing optical sight (LCOS) systems in performing the air-to-air tracking task, fighter-on-fighter.

Most studies in the past, such as the many "Paper Pilot" (Ref 1) investigations have utilized the quasi-linear pilot describing function models as formulated by McRuer (Ref 14). However, the present study uses the optimal pilot describing function model formulated by Kleinman, Baron, Miller, Elkind, and Levison, hereafter referred to as the "Kleinman model" (Ref 2). This model incorporates a Kalman filter and state predictor to simulate the analytical and anticipatory tasks which a pilot must perform to properly control an aircraft. Kleinman has shown that this model very accurately represents the response of a pilot in performance of a number of tasks, such as the landing approach (Ref 8), helicopter hover (Ref 2), and ground-based anti-aircraft gunnery (Ref 10).

The Analysis Procedure

To show that the Kleinman pilot model does indeed exhibit

performance characteristics closely matched to those of a human pilot in the air-to-air tracking task, two separate simulations are required. First, data must be gathered on actual pilot performance in this task. That is accomplished in this study by simulating the task on an analog computer and presenting it to three pilots with previous fighter aircraft experience. This presentation is done via a fixed-base simulator to be described in Section III. The data thus collected reflect pilot workload and performance of the task confronting him in each experimental case.

The second simulation pits the Kleinman model against the identical tasks on the CDC 6600 digital computer. The same statistical data on workload and performance are collected from the simulation and compared with that obtained from the analog simulation. The results of this comparison are revealed in Section V of this report.

To obtain a large enough spread in the data to accentuate the correlation between analog and digital results, several different aircraft, ranging from good to bad aerodynamic designs for this task, are used at varying altitudes and Mach number. Additionally, for each aircraft, two different tracking ranges and two different target RMS "G" loadings are simulated.

Limits and Assumptions

The dynamics of the air-to-air combat tracking task are extremely complex when considered from a three-dimensional aspect. This is due primarily to the inertial cross-coupling

of the aircraft longitudinal, lateral, and yaw axes that manifests itself in the aircraft equations of motion. So, as a starting point in the analysis of this problem, this study is limited to an analysis of the longitudinal tracking task only, and neglects any cross-coupling effects. This procedure is common practice and usually lends itself to realistic results. Future work should concentrate on expansion of this study to three dimensions.

It is further assumed that the problem begins with the attacking aircraft already in a tracking position relative to the target aircraft; thus the task is "merely" to continue tracking the target as closely as possible. The attacking aircraft is considered to be rigid and impervious to "G" loadings in excess of normal maximums in the interest of tracking the target with minimum error. Also, it is assumed that the attacking aircraft possesses the capability of producing infinite thrust and can therefore maintain constant Mach number under any conditions of G-loading, angle of attack, or attitude. Since the Kleinman pilot model is basically a linear regulator, all dynamic equations in the study have been linearized about the aircraft stability axis, and perturbations are assumed small enough to validate the use of these linear equations in a nonlinear environment. In addition, the aircraft stability derivatives are assumed constant throughout the tracking task, an assumption which, in the light of assumed constant Mach number, is quite valid.

Finally, the affects of gravity on this problem contribute

only bias terms that merely complicate the equations and computations. Therefore, these affects are neglected, and any reference to "G" forces in this text alludes only to kinematic accelerations.

II. The Air-To-Air Tracking Task

Modelling the Sight Dynamics

The task of accurately tracking a maneuvering target for the purpose of obtaining a "kill" with airborne cannon fire is one of the most difficult required of a fighter pilot. As is the case when firing any projectile at a moving target, lead for target motion must be computed and the aiming direction adjusted to compensate accordingly. Further complicating the air-to-air problem are trajectory adjustments that must be made to account for projectile drag, velocity jump, and gravity drop, as well as other more minor effects. The total compensation is normally presented to the pilot of the attacking aircraft in the form of a two-mils-in-diameter "pipper", surrounded by a larger circle called the reticle, and depressed from the weapon line by the amount of this computed lead angle, as is shown in Figure 1. Thus, when the pilot maneuvers his aircraft in such a manner as to place the "pipper" on the target, he has achieved the proper aiming direction to insure a kill should the target maneuver remain constant.

Neglecting windage jump and the effects of gravity, the lead angle required is, in general, computed from the following vector equation (Ref 18:7-8):

$$\underline{\lambda} = \frac{D}{V_f}\,\dot{\underline{\Sigma}}_T + \frac{T_f}{2V_f}\,(\underline{s} \times \dot{\underline{V}}_T) - J_v\,\frac{V_A}{V_f}\,\underline{\alpha} \qquad (1)$$

where

$\underline{\lambda}$ = vector lead angle

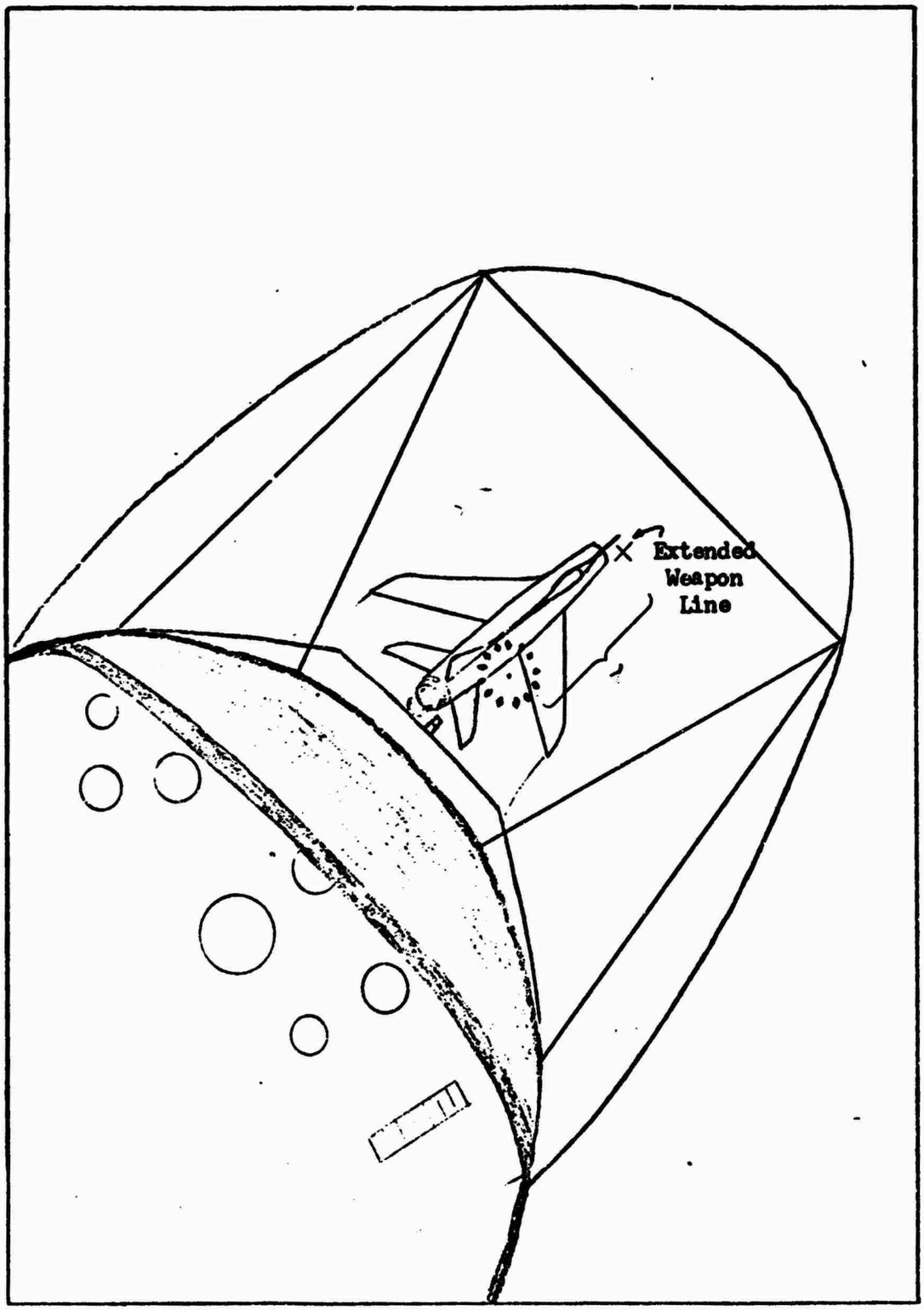

Figure 1. Air-To-Air Tracking As Seen By Pursuing Pilot At Close Range (Approximately 1000 Feet).

D = present range

V_f = mean relative velocity of projectile over one time of flight

$\dot{\underline{\Sigma}}_T$ = inertial angular rate of line of sight (LOS) from the attacker to the target

T_f = time of flight to target future position

$\underline{s}$ = unit vector along the LOS

$\dot{\underline{V}}_T$ = vector acceleration of target along vertical (positive down)

J_v = ballistic jump parameter

V_A = attacker velocity magnitude

$\underline{\alpha}$ = angle of attack

The first term in this equation is that portion of the lead angle that compensates for linear target motion. The second term accounts for target acceleration across the line of sight, the vector cross-product being the component of target acceleration normal to the LOS. The last term adjusts the lead angle for initial trajectory errors due to attacker angle of attack at the instant of firing.

Figure 2 portrays the principle angle relationships in the in-plane, air-to-air tracking situation. Since the LOS rate ($\dot{\underline{\Sigma}}_T$) cannot be directly measured by the attacking aircraft, it is approximated in the LCOS system by $\dot{\underline{\Sigma}}_p$, the inertial angular rate of the reticle, or pipper. This approximation is good so long as the sight is held exactly on the target. However, when the attacker is maneuvering to put the sight on the target, or the target does not remain in a constant maneuver, $\dot{\underline{\Sigma}}_p$ is not equal to $\dot{\underline{\Sigma}}_T$, and the computed lead angle will be in error until steady

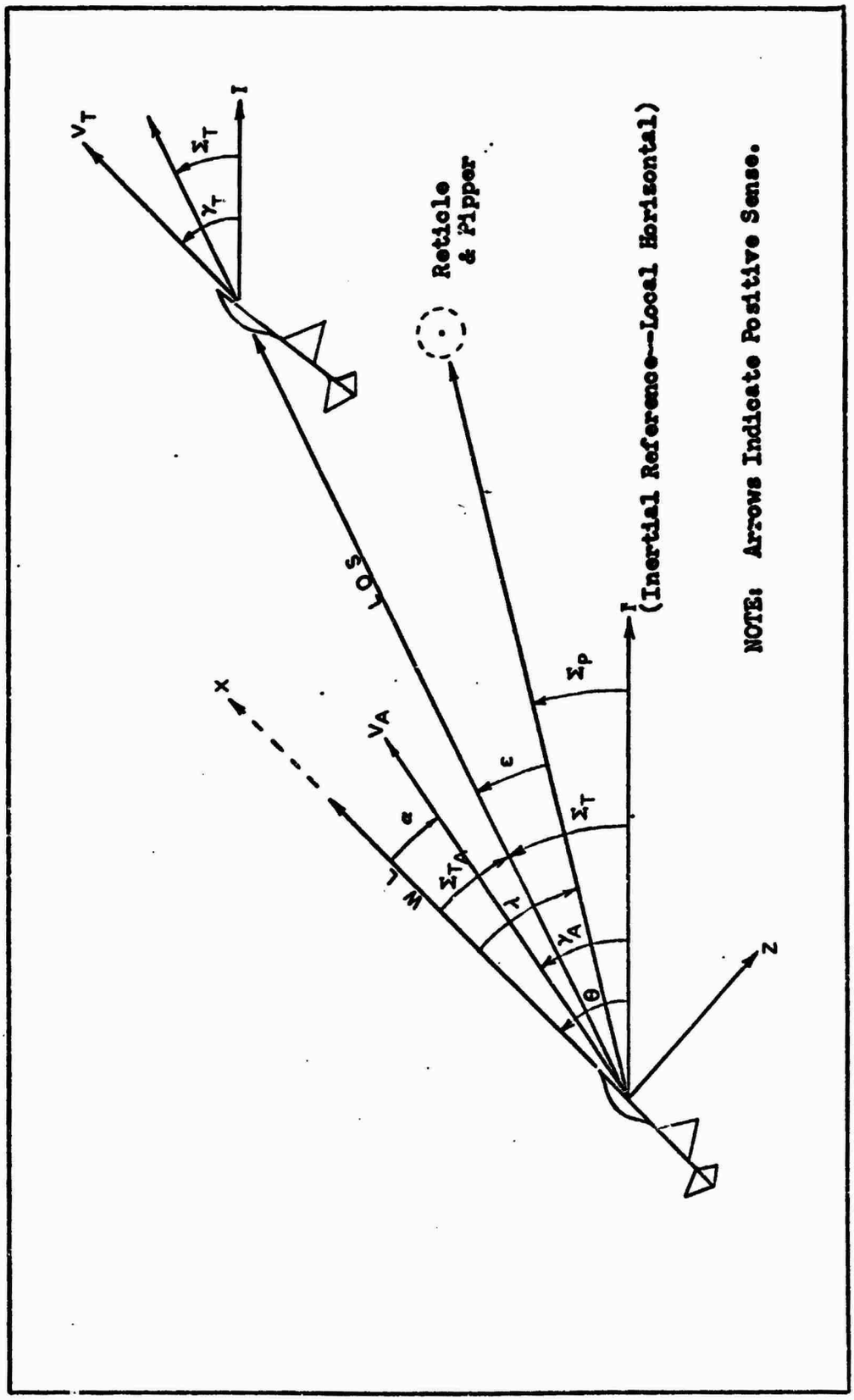

Figure 2. Air-To-Air Tracking Geometry.

tracking is achieved. From Figure 2, it can be seen that

$$\underline{\Sigma}_p = \underline{\theta} - \underline{\lambda} \tag{2}$$

so, assuming $\dot{\underline{\Sigma}}_p = \dot{\underline{\Sigma}}_T$,

$$\dot{\underline{\Sigma}}_p = \dot{\underline{\theta}} - \dot{\underline{\lambda}} = \dot{\underline{\Sigma}}_T \tag{3}$$

Substituting (3) into (1):

$$\underline{\lambda} = \frac{D}{V_f}(\dot{\underline{\theta}} - \dot{\underline{\lambda}}) + \frac{T_f}{2V_f}(\underline{s} \times \dot{\underline{V}}_T) - J_v \frac{V_A}{V_f} \underline{\alpha} \tag{4}$$

In this analysis, target range remains constant throughout the tracking time; i.e., there is no closure rate, so the attacker is "camped" on the target. So, since the muzzle velocity of the projectile, V_m, normally is much greater than the velocity of the attacker, V_A,

$$\frac{D}{V_f} \approx T_f \tag{5}$$

Equation (4) can thus be rewritten

$$\dot{\underline{\lambda}} = -\frac{1}{T_f}\underline{\lambda} + \dot{\underline{\theta}} + \frac{1}{2V_f}(\underline{s} \times \dot{\underline{V}}_T) - J_v \frac{V_A}{V_f T_f} \underline{\alpha} \tag{6}$$

Now, since $\dot{\underline{V}}_T$ is also unknown, the quantity $(\underline{s} \times \dot{\underline{V}}_T)$ can be approximated by $(\underline{s} \times \underline{A}_{n_A})$, where $\underline{A}_{n_A}$ is the normal acceleration of the attacking aircraft (Ref 18:10). From linear perturbation theory (Ref 4:16)

$$|\underline{A}_{n_A}| = -\dot{\gamma}_A V_A \tag{7}$$

and, from Figure 2

$$\gamma_A = \theta - \alpha \tag{8}$$

so,

$$\dot{\gamma}_A = \dot{\theta} - \dot{\alpha} \tag{9}$$

But (Ref 4:14-21)

$$\dot{\theta} = q \tag{10}$$

and

$$\dot{\alpha} = q + Z_\alpha \alpha + Z_\delta \delta \tag{11}$$

Therefore, substituting (10) and (11) into (9)

$$\dot{\gamma}_A = - Z_\alpha \alpha - Z_\delta \delta \tag{12}$$

and

$$|\underline{A}_{n_A}| = V_A (Z_\alpha \alpha + Z_\delta \delta) \tag{13}$$

Now, in the high "G", high angle-of-attack environment that exists under aerial dogfight conditions,

$$Z_\delta \delta << Z_\alpha \alpha \tag{14}$$

so the left-hand term can be neglected and

$$|\underline{A}_{n_A}| \simeq V_A Z_\alpha \alpha \tag{15}$$

This gives

$$\underline{s} \times \underline{A}_{n_A} = - V_A Z_\alpha \underline{\alpha} \sin(\lambda + 90°) \tag{16}$$

$$= - V_A Z_\alpha \underline{\alpha} \cos \lambda \tag{17}$$

using small angle approximations:

$$\underline{s} \times \underline{A}_{n_A} = - V_A Z_\alpha \underline{\alpha} \tag{18}$$

Substituting this result back into (6): for $(\underline{s} \times \dot{\underline{V}}_T)$

$$\dot{\underline{\lambda}} = - \frac{1}{T_f} \underline{\lambda} + \underline{q} - \frac{V_A Z_\alpha}{2 V_f} \underline{\alpha} - J_v \frac{V_A}{V_f T_f} \underline{\alpha} \tag{19}$$

or combining terms and dropping the vector notation

$$\dot{\lambda} = - \frac{1}{T_f} \lambda + q - \frac{V_A}{V_f} \left(\frac{Z_\alpha}{2} + \frac{J_v}{T_f} \right) \alpha \tag{20}$$

This is the equation that is instrumental in the LCOS system to position the pipper at the current correct aiming point on the pilot's "heads-up" display.

Velocity Jump Correction

J_v, the velocity jump correction angle, is illustrated in Figure 3. It is a consequence of the fact that the projectile muzzle velocity vector and the aircraft velocity vector are not normally colinear when the aircraft is being maneuvered, and is calculated from (Ref 20:47)

$$J_v = \frac{\underline{V}_A \times \underline{l}_{(WL)}}{|\underline{V}_p|} = \frac{V_A \sin \alpha}{V_A + V_m} \tag{21}$$

where $\underline{l}_{(WL)}$ = unit vector directed along the weapon line.

Assuming small angles

$$J_v \approx \frac{V_A \alpha}{V_A + V_m} \tag{22}$$

Because it is a function of angle of attack (α), the jump correction function had to be linearized about a nominal angle of attack in order to render equation (20) linear. This nominal value was chosen as 10° in all cases.

Short-Comings of the LCOS System

Once the attacker is in a tracking position on the target (normally behind and slightly elevated in the target's plane of motion), he must then generate an angular rate of turn in that plane approximately equal to that of the target. The major tracking problem with the LCOS system arises when the attacker does not have the sight on the target. For instance, if the sight is behind the target the pilot must

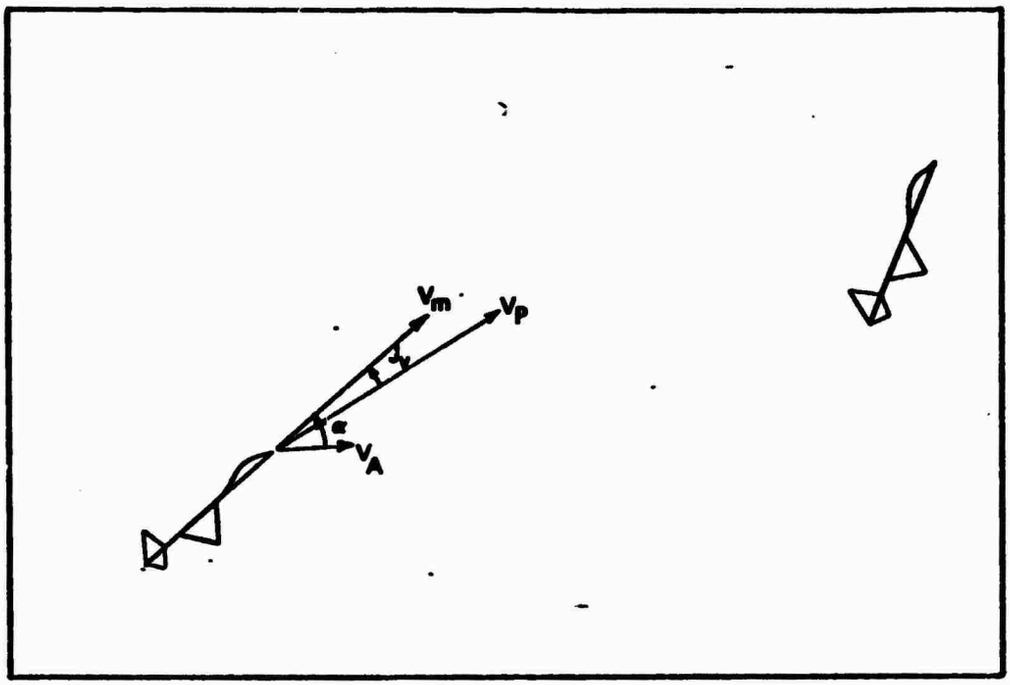

Figure 3. Velocity Jump Correction Geometry

increase his turn rate to catch up. This results in an erroneous increase in the displayed lead angle, leaving the pilot with no valid information as to exactly where to position his aircraft until his rate of turn is once again constant and equal to that of t e target. A process of "hunting" then ensues until the pilot has either found the exact solution or decides to hold one solution steady and fire continuously while allowing the sight to "slide through" the target. In practice, the latter procedure usually leads to the best results. As is evident from equation (20), as range increases, the sight time constant, T_f, becomes larger, causing these unwanted dynamics to become even worse. Normally, the sight is designed with a nominal time constant based upon a nominal firing range of around 1500 feet (Ref 5:1-1).

In Appendix A it is pointed out that the sight time constant for each case in this study was computed based upon the given tracking conditions.

Kinematics

The inertial line of sight from the attacker to the target is computed from (Ref 18:11)

$$\dot{\underline{\Sigma}}_T = \frac{1}{D} [\underline{s} \times \underline{V}_T - \underline{s} \times \underline{V}_A] \tag{23}$$

which states that the inertial rate of rotation of the LOS is given by the difference between the relative angular rates of rotation of the target and the attacker. From Figure 2 this equation becomes, considering the in-plane task only

$$\dot{\Sigma}_T = \frac{V_T}{D} \sin(\gamma_T - \Sigma_T) - \frac{V_A}{D} \sin(\lambda-\alpha-\epsilon) \tag{24}$$

Using small angle assumptions and noting from Figure 2 that

$$\epsilon = \Sigma_T - \Sigma_p = \Sigma_T - \theta + \lambda \tag{25}$$

$$\dot{\Sigma}_T = \frac{V_T}{D} (\gamma_T - \Sigma_T) - \frac{V_A}{D} (\theta-\alpha-\Sigma_T) \tag{26}$$

or

$$\dot{\Sigma}_T = \frac{V_A}{D} \alpha + \frac{V_A-V_T}{D} \Sigma_T + \frac{V_T}{D} \gamma_T - \frac{V_A}{D} \theta \tag{27}$$

Since allowing a rate of change of range, D, would render the equations nonlinear, the cases considered in this study were limited to zero closure rate with the velocities of the attacker and target constant and equal. Therefore, the second term in (27) was always zero in this study.

III. Analog Simulation of the Air-to-Air Task

The purpose of the analog computer simulation was to gather appropriate data on specific performance functions to compare with similar results from digital computer runs of the identical tasks "flown" by the analytical pilot model. A system model of this task can be broken up into five functional areas, as shown in Figure 4: the pilot (or pilot model), the flight control response, the aircraft equations of motion, the sight computer, and the kinematics of the problem. The system variables chosen as the states which fully describe the task were the attacking aircraft's elevator deflection, δ, pitch angle, θ, pitch rate, q, and angle of attack, α; the lead angle, λ, the inertial line of sight from the attacker to the target, Σ_T; the normal acceleration of the target, A_{n_T}; the flight path angle of the target, γ_T; and a dummy state representing the first stage filtering of white, Gaussian noise.

The Attacker Model

Equations of Motion. As was mentioned previously in the introduction to this text, the equations of motion of the attacking aircraft were approximated by the standard "short-period" stability axis equations. These equations are first-order, linear, and, in view of the assumption of constant stability derivatives, time-invariant differential equations which approximate aircraft response to control inputs. Since this analysis is concerned only with the longitudinal

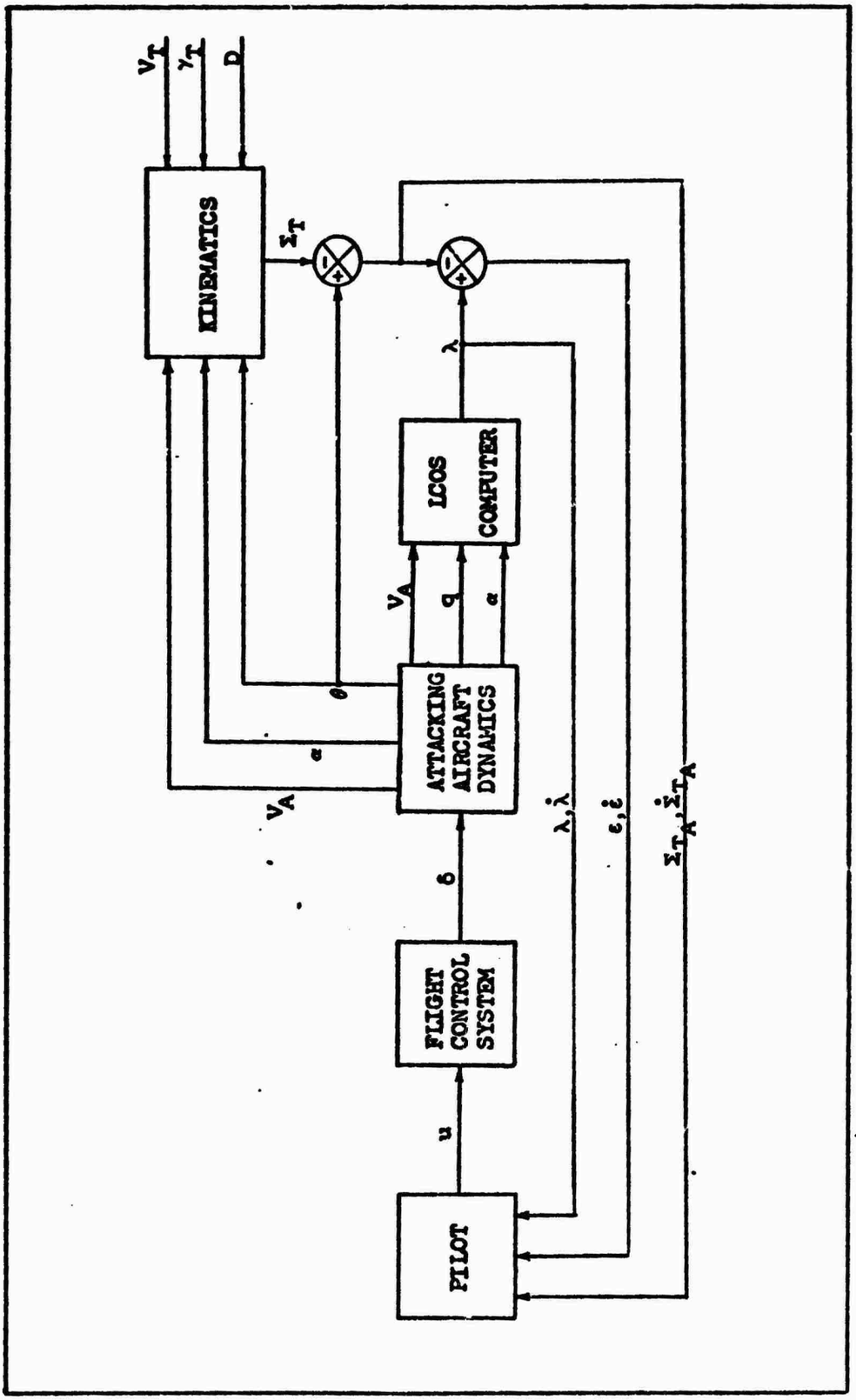

Figure 4. Functional Diagram of the Two-Dimensional Air-To-Air Tracking Task.

axis dynamics, only three equations are necessary. Those describing pitch angle and angle of attack were presented in Section II as equations (10) and (11), respectively. The third equation, that for pitch rate is (Ref 4:14-21)

$$\dot{q} = M_q q + M_\alpha \alpha + M_{\dot{\alpha}} \dot{\alpha} + M_\delta \delta \tag{28}$$

substituting (11) in (28) and rearranging

$$\dot{q} = (M_\delta + M_{\dot{\alpha}} Z_\delta)\delta + (M_q + M_{\dot{\alpha}})q + (M_\alpha + M_{\dot{\alpha}} Z_\alpha)\alpha \tag{29}$$

Elevator Actuation. The transfer function relating elevator deflection, δ, to commanded elevator deflection, δ_c, for a typical tactical fighter aircraft is given by (Ref 19:155)

$$\frac{\delta}{\delta_c} = \frac{K_L}{1 + \tau_a s} \tag{30}$$

where K_L is the control linkeage gain and τ_a is the time constant of the power cylinder actuator. Typical values for these two parameters are 0.8 (dimensionless) and 0.05 seconds, respectively. The differential equation for elevator deflection is then

$$\dot{\delta} = -\frac{1}{\tau_a}\delta + \frac{K_L}{\tau_a}\delta_c \tag{31}$$

The analog simulation utilizes a force stick that converts pilot pressure in pounds to volts, where one volt equals 0.01 radian in the scaled circuitry. The equation modelled in the circuitry is (Ref 3:12)

$$-\delta_c = K_f F_s \tag{32}$$

where K_f is the force stick sensitivity in units of radians

per pound, and F_s is the applied force in pounds. The negative sign on δ_c is a consequence of the fact that positive elevator deflection is commonly defined in the aircraft equations of motion as that movement which results in a negative pitch rate; i.e., "down" elevator. Substitution of (32) into (31) then gives

$$\dot{\delta} = -\frac{1}{\tau_a}\delta + \frac{K_L K_f}{\tau_a} F_s \qquad (33)$$

Figure 5 is the analog schematic of the attacking aircraft dynamics. Note that a stick sensitivity adjustment potentiometer was included in the factors making up K_f. This "pot" was located on the instrument panel of the simulated aircraft cockpit so that the pilot could adjust the stick sensitivity to an optimum level for his technique. This was done so that limitations on stick "feel" would not be a factor in each pilot's performance of the task.

Target Modelling

Generation of Target Motion. The target aircraft was a fighter aircraft possessing capabilities at least as strong as those of the pursuer. Target normal acceleration, A_{n_T}, was derived from band-limited, Gaussian white noise with statistics of zero mean and standard deviations (RMS) of 3.5G and 5.0G for each case tested. The analog schematic of Figure 6 was used to record target motion for purposes of repetitive use. The output of a Gaussian white noise generator was subjected to a double filter network to obtain a random function which represented

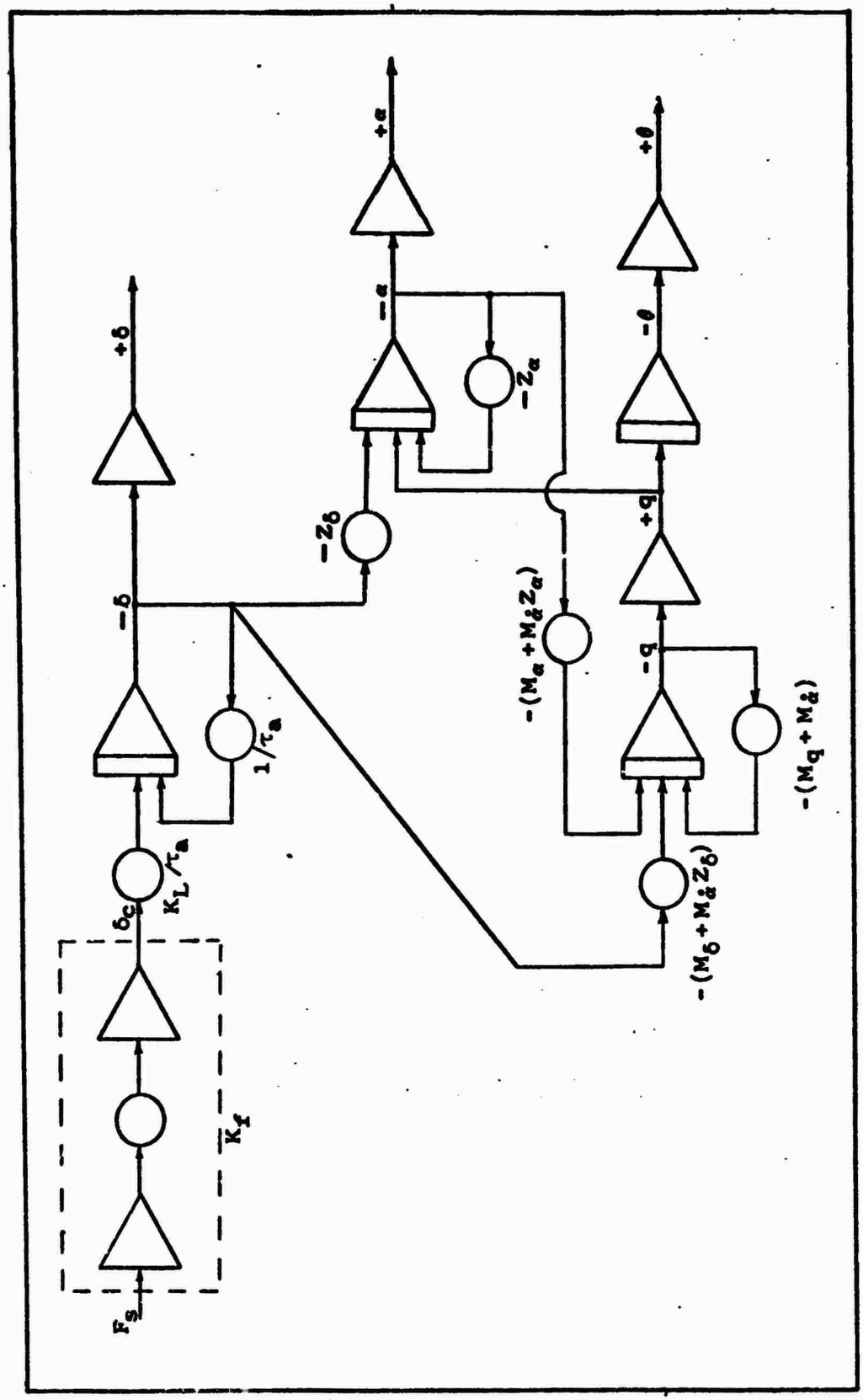

Figure 5. Analog Schematic of the Attacker Aircraft Dynamics.

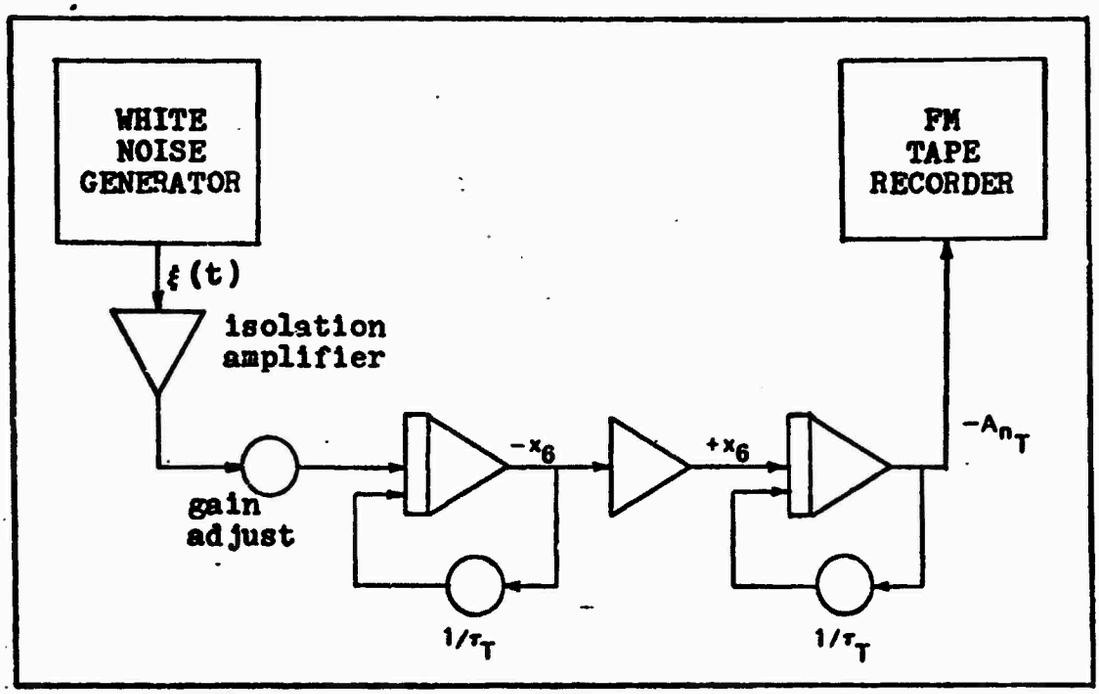

Figure 6. Analog Circuit for Taping Target Motion

"realistic" target motion. The break frequency, $1/\tau_T$, was manipulated by trial and error until this "realistic" motion was obtained. A value of τ_T equal to 3 seconds was found to be best for this situation. It was quickly discovered that, even though the tape recorded "motion" of the target was completely random, characteristic peaks in the function were easily remembered by the test pilots, and, after a few runs, even anticipated. To alleviate this problem, three separate target motions were recorded and used in each case. Figure 7 shows reproductions of the three target motions used.

Target Interface with the System. Recall from Section II that equation (27) called for a knowledge of the target flight path angle, γ_T. It should be noted here that this parameter is used explicitly in this study only because it

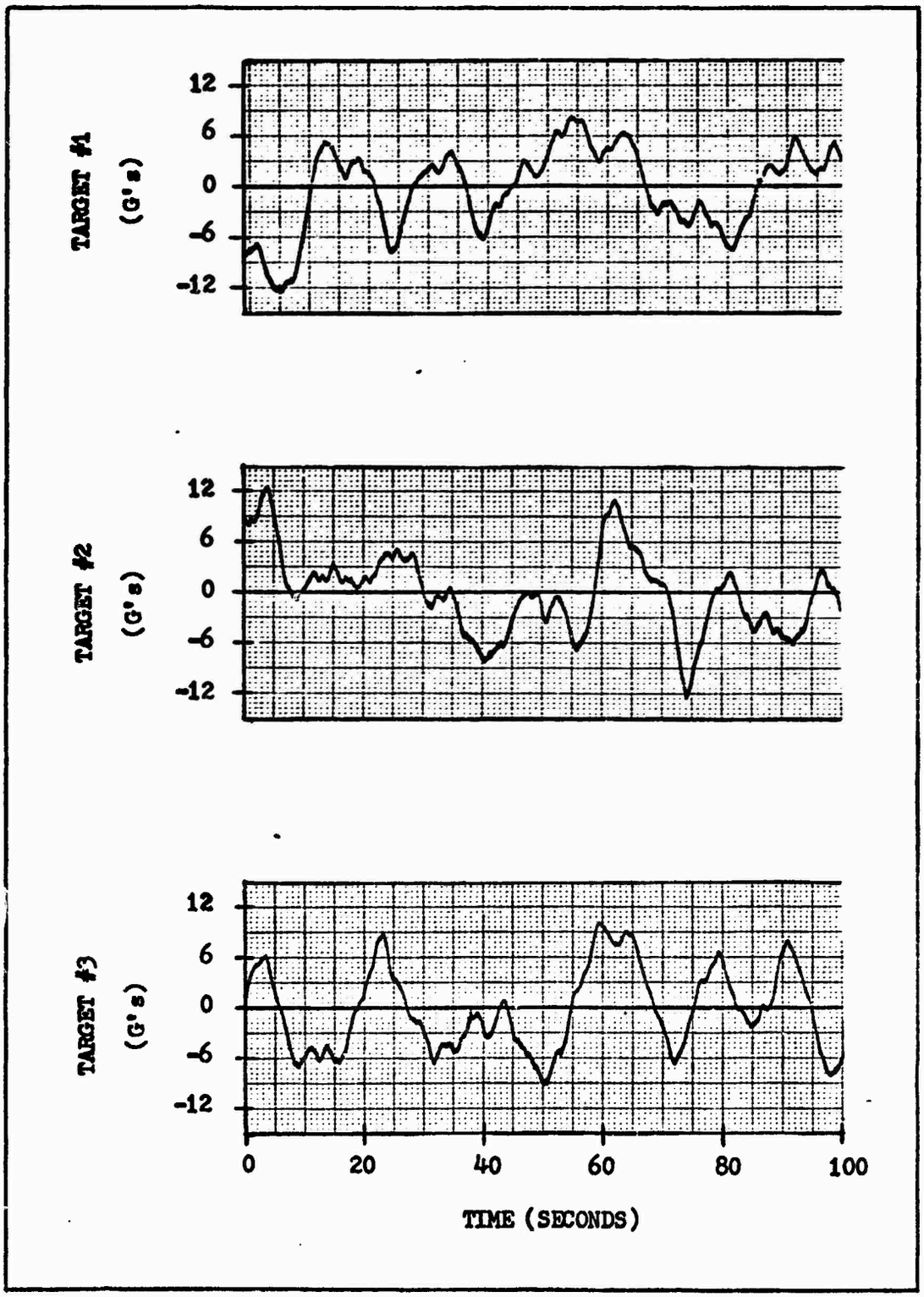

Figure 7. Time History of Target Acceleration.

is available in the simulation. In reality it would be approximated by own ship's flight path angle. However, since it is available in the simulation and since, as with equation (7)

$$A_{n_T} = - \dot{\gamma}_T V_T \tag{34}$$

then

$$\dot{\gamma}_T = - \frac{1}{V_T} A_{n_T} \tag{35}$$

Figure 8 is the analog schematic of target motion input to the system dynamics, specifically, the $\dot{\Sigma}_T$ equation. The bias circuitry was necessitated by the requirement for zero mean motion (see Section IV), and the gain adjustment was to facilitate changing RMS "G" levels. The "$1/V_T$" term in (35) forced normalization of the equations since that term was quite small in magnitude and would have effectively blocked

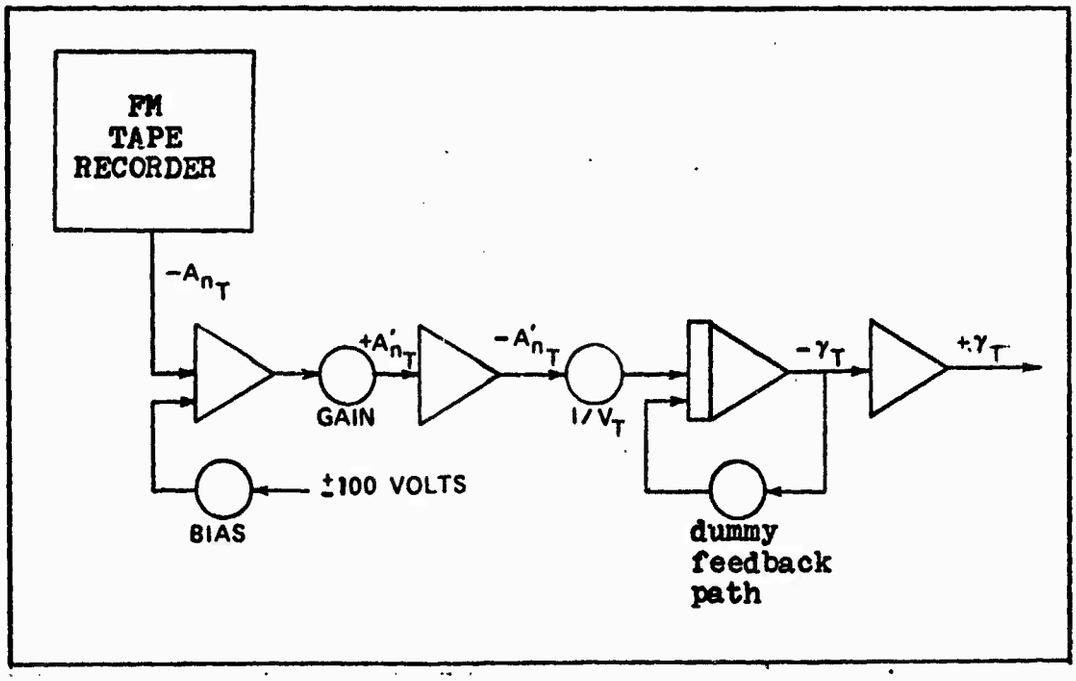

Figure 8. Analog Circuit for Target Flight Path Angle Generation

the target signal from reaching the rest of the system. One thousand feet was chosen as one distance unit (DU) in the normalized equations, with one second remaining one time unit (TU). Consequently, one velocity unit (VU) became 1000 ft/sec and one acceleration unit was 1000 ft/sec^2. Though it does not appear in the equation, a dummy feedback path was added to the $\dot{\gamma}_T$ equation to keep the steady state covariance of γ_T from becoming infinite (see Section IV). A nominal value of 0.01 was used for this feedback path so that it would have little, if any, affect on the actual dynamics beind modelled.

Sight Dynamics and Problem Kinematics

The lead angle and line of sight angle equations were derived in Section II as equations (20) and (27), respectively. The analog models of these equations are shown in Figure 9. Also shown are the circuits for the computation of Σ_{T_A}, the relative line of sight of the target with respect to the attacker weapon line, and ε, the tracking error. The mathematical relationships for these last two parameters were derived from the geometry of Figure 2 as

$$\Sigma_{T_A} = \theta - \Sigma_T \tag{36}$$

and

$$\varepsilon = \lambda - \Sigma_{T_A} \tag{37}$$

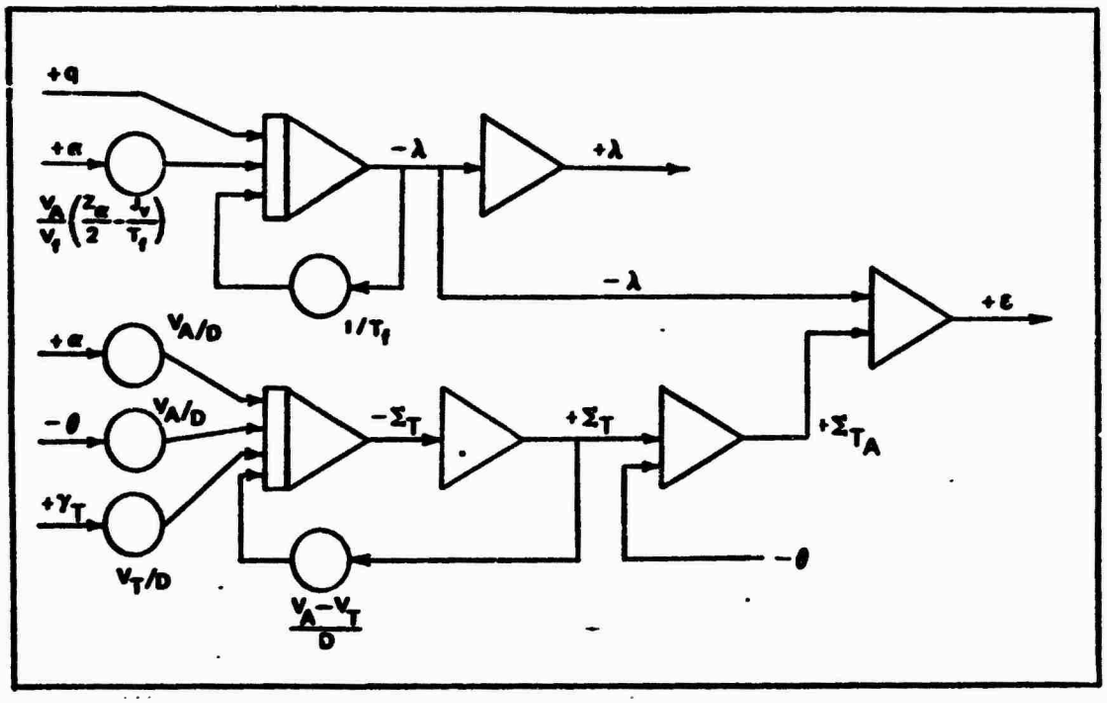

Figure 9. Analog Representation of Sight and Problem Kinematics

The Fixed-Base Simulator

Figure 10 is a photograph of the simulator "cockpit". It consists of a fighter aircraft ejection seat with side-stick controller and a dual-beam cathode ray oscilloscope upon which the task is displayed mounted at eye level. The side-stick controller is similar to that being used in one advanced, light-weight fighter "fly-by-wire" design. In the simulation, the stick is trimmed for level flight and cannot be retrimmed.

Presentation of the Task to the Pilot. When tracking a target, the pilot of the pursuing aircraft is aware primarily of two parameters: the position of the target and the position of the sight. The difference between the two positions is the tracking error, and this is what the pilot attempts to minimize. In this simulation, the target is

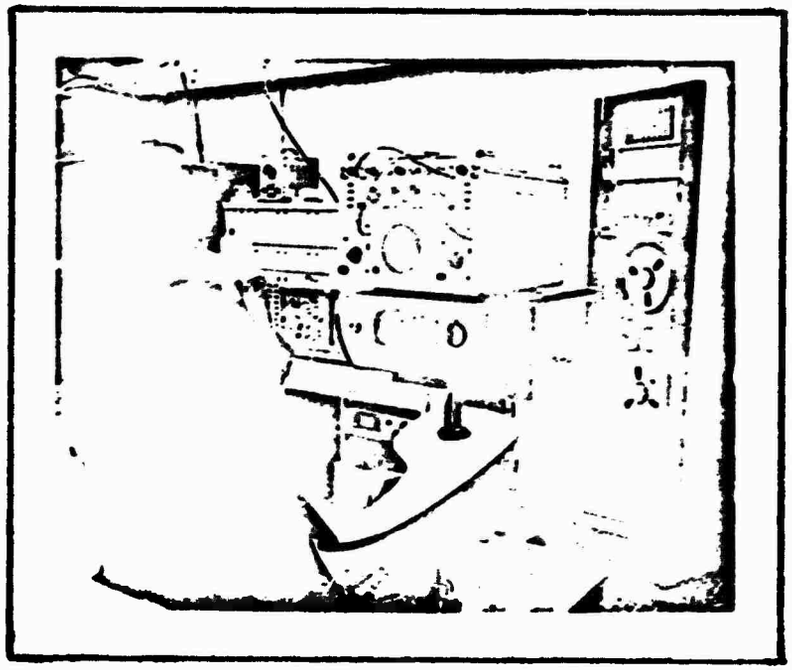

Figure 10. The Fixed-Base Simulator

displayed on the oscilloscope as an inverted "T". It is positioned relative to the center of the oscilloscope, assumed to be the extension of the aircraft's weapon line, by the current magnitude of Σ_{T_A}, the relative line of sight to the target. The sight is positioned relative to the center of the oscilloscope by the current magnitude of λ, the lead angle. Figure 11 illustrates the picture seen by the pilot. The tracking error shown is positive; i.e., the attacker is lagging behind the target. Note that only the reticle portion of the sight is represented. This is due to the limitations encountered on being able to physically generate both the reticle and the pipper, as well as the target symbol, on the same oscilloscope at the same time. The pilots thus had to estimate the position of the center

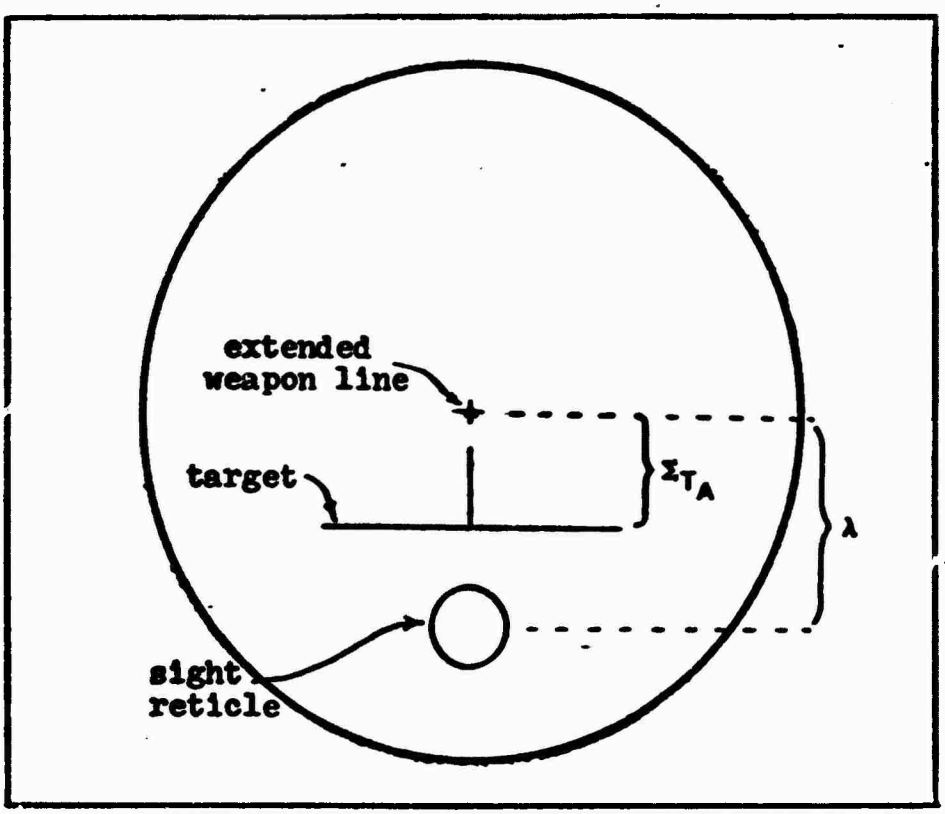

Figure 11. Simulation Display

of the reticle to achieve zero-error tracking.

The Gathering of Data. After an extended period of training during which the three pilots became used to the task before them and the feel of the side-mounted, force-stick controller, the taking of data began. Twelve separate cases were run using three different aircraft dynamics, two ranges, and target RMS G levels of 3.5G's and 5.0G's. The three aircraft were the F-4E, the F-5, and the A-7. A summary of the dynamics of each aircraft is presented in Table I. Ranges of 3000 feet and 1000 feet were decided upon since they represent approximate maximum and minimum tracking ranges in an actual situation. As was mentioned previously, three different recorded target motions possessing identical

Table I.

Dynamic Parameters and Stability Derivatives

Aircraft	F-4E†	F-5*	A-7*
Altitude (Ft)	15,000	5,135	15,000
Mach Number	0.90	0.81	0.60
Velocity, V_o (Ft/Sec)	951.6	889.0	635.0
Dynamic Pressure, q_o (Lb/Ft^2)	677.3	804.4	301.0
Mass, m (Slugs)	1433.5	354.0	680.0
Reference Area, S (Ft^2)	530.0	170.0	375.0
C_{L_α} (1/Rad)	- -	3.95	4.40
C_{L_δ} (1/Rad)	- -	0.859	0.600
Z_α** (1/Sec)	-1.0326	-1.7164	-1.1502
Z_δ** (1/Sec)	-0.09512	-0.3733	-0.1568
M_α ($1/Sec^2$)	-10.443	-10.30	-9.08
$M_{\dot{\alpha}}$ (1/Sec)	-0.3439	-0.0646	-0.133
M_q (1/Sec)	-0.7381	-1.350	-0.696
M_δ ($1/Sec^2$)	-37.08	-47.2	-18.90

† (Ref 7:80-81)

* (Ref 17:146,148)

** Values for Z_α and Z_δ for the F-5 and the A-7 were calculated from

$$Z_\alpha = -\frac{q_o S}{mV_o} C_{L_\alpha}$$

$$Z_\delta = -\frac{q_o S}{mV_o} C_{L_\delta}$$

statistics were used in each case. Thus, each pilot "flew" a minimum of 36 times once data-gathering runs began.

A typical data run began with the target and the sight both stationary in the center of the screen, making all initial conditions equal to zero. The picture thus displayed represented a situation in which, unbeknown to the target, the attacker had maneuvered into a stern, or "6 o'clock", attack position. When the pilot was ready, a switch was thrown to activate the problem dynamics with no target motion other than that generated by the action of the attacker pilot. Shortly thereafter, a second switch was thrown sending the taped target motion to the display. This simulated sudden target awareness of the attacker's approach followed by high "G" evasive action. At a predetermined point on the tape a switch was thrown to start the data measurement circuitry. For 100 seconds thereafter, analog integrators evaluated the time integrals of elevator deflection, δ, pitch rate, q, lead angle, λ, the relative line of sight of the target, Σ_{T_A}, tracking error ε, attacker normal acceleration, A_{n_A}, and target motion, as well as the squares of all of these variables. An example of a typical run as recorded on the strip chart is shown in Figure 12.

Data Recorders

Since the target motion is filtered Gaussian white noise and the system is linear, the statistics of the system states are assumed to be stationary and ergotic and the mean and

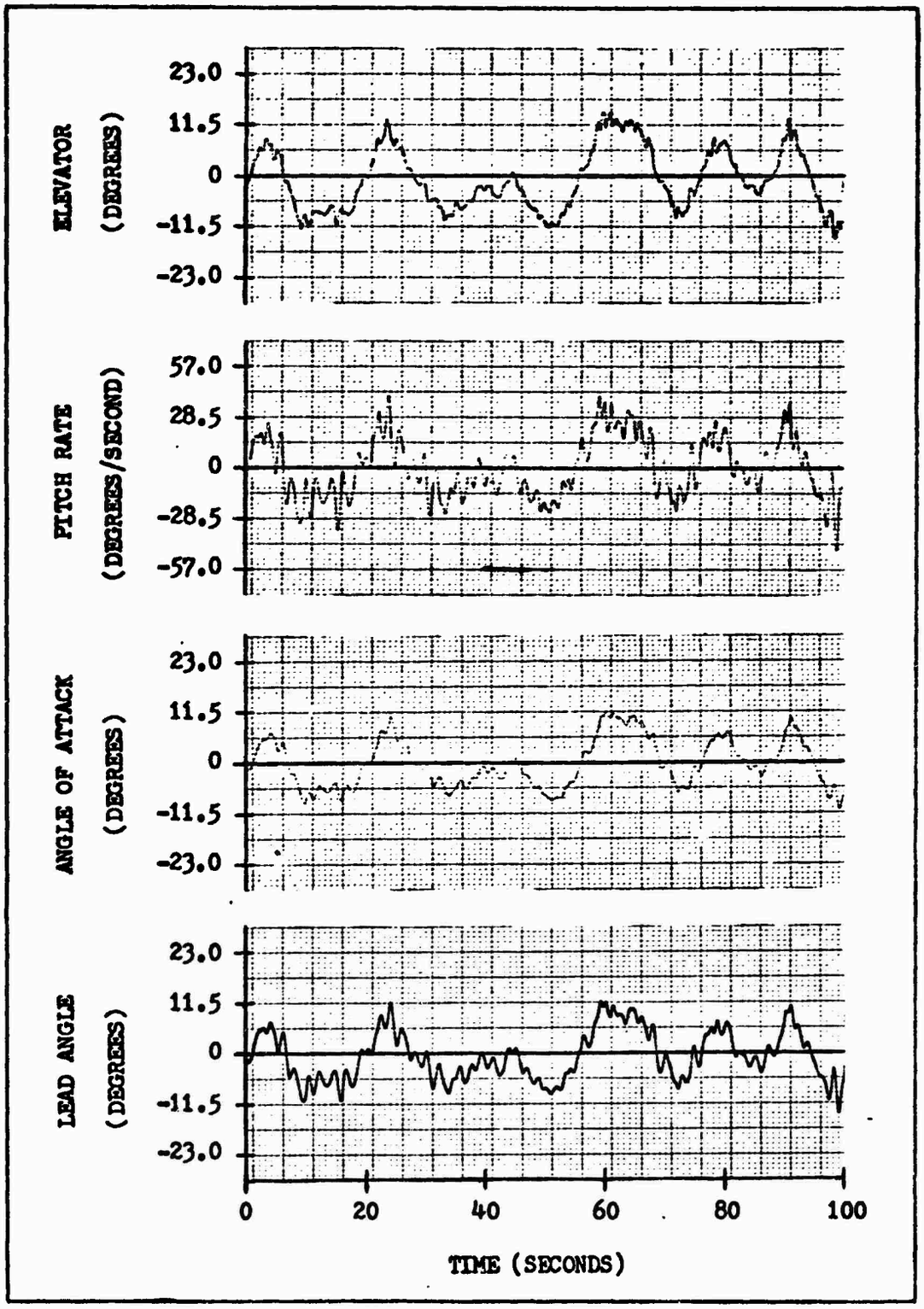

Figure 12a. Typical Tracking Performance: Range - 1000 Feet, 5 G Target.

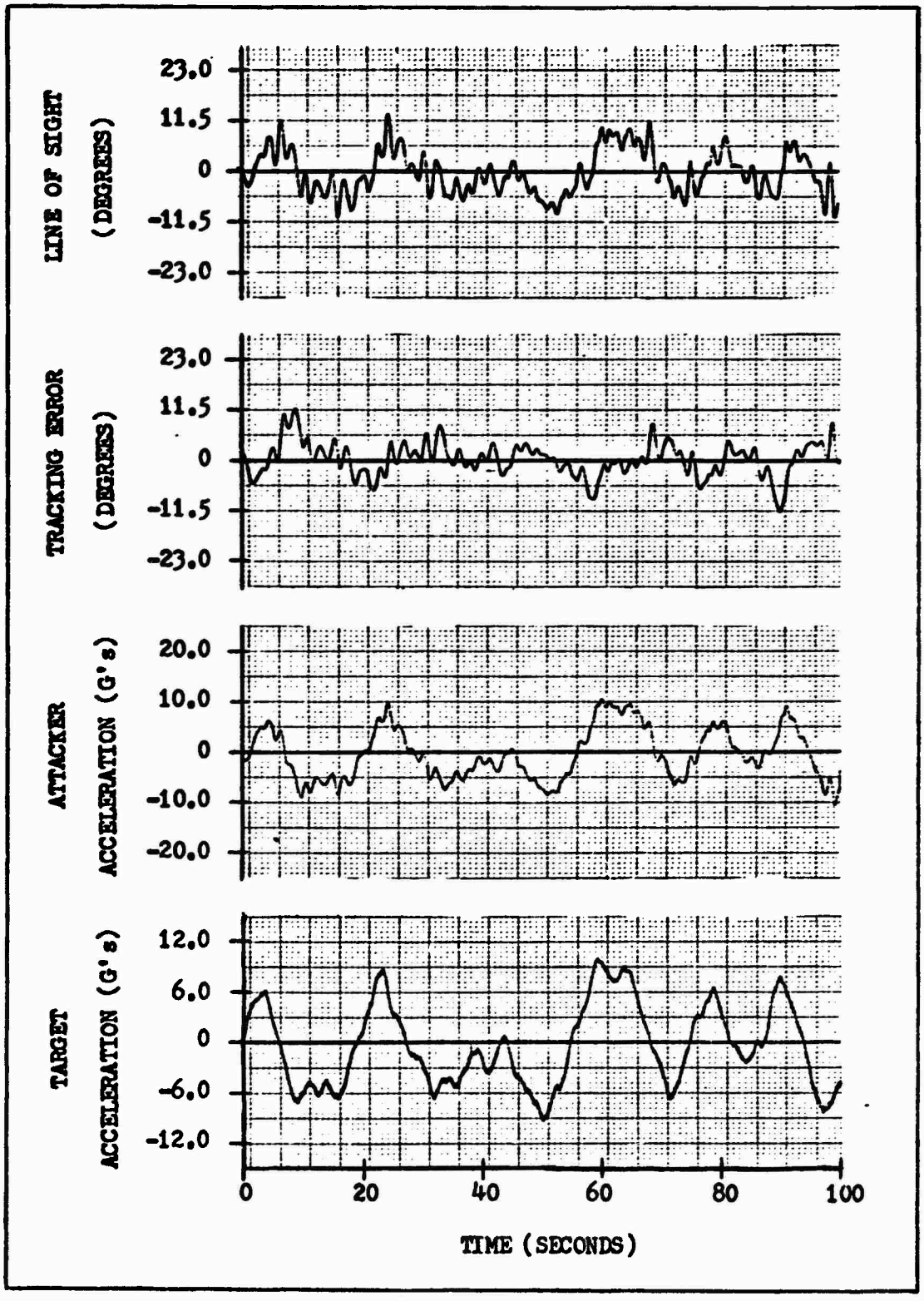

Figure 12b. Typical Tracking Performance: Range - 1000 Feet, 5 G Target.

autocorrelation functions can be approximated by (Ref 16:82)

$$E\{x\} \approx \frac{1}{T} \int_0^T x \, dt \tag{38}$$

$$E\{x^2\} \approx \frac{1}{T} \int_0^T x^2 \, dt \tag{39}$$

The variance is then

$$\sigma_x^2 = E\{[x - E\{x\}]^2\} \tag{40}$$

$$= E\{x^2\} - [E\{x\}]^2 \tag{41}$$

The RMS value, or standard deviation, of each state is then the square root of the variance. Thus, after each 100-second run, the outputs of the fourteen aforementioned integrators were recorded and properly manipulated using equations (38), (39), and (41) to determine the standard deviation of each state measured. These were recorded for later comparison with the digital pilot analysis.

Figure 13 shows the analog circuitry used to evaluate equations (38) and (39). The potentiometers were needed for scaling purposes to prevent amplifier overloads.

The complete, tabulated results of the analog simulation are attached to this report as Appendix B. A discussion of the results is contained in Section V. A summary of the flying experience of the pilots who flew the simulation as well as some of their comments pertinent to this study is included as Appendix C.

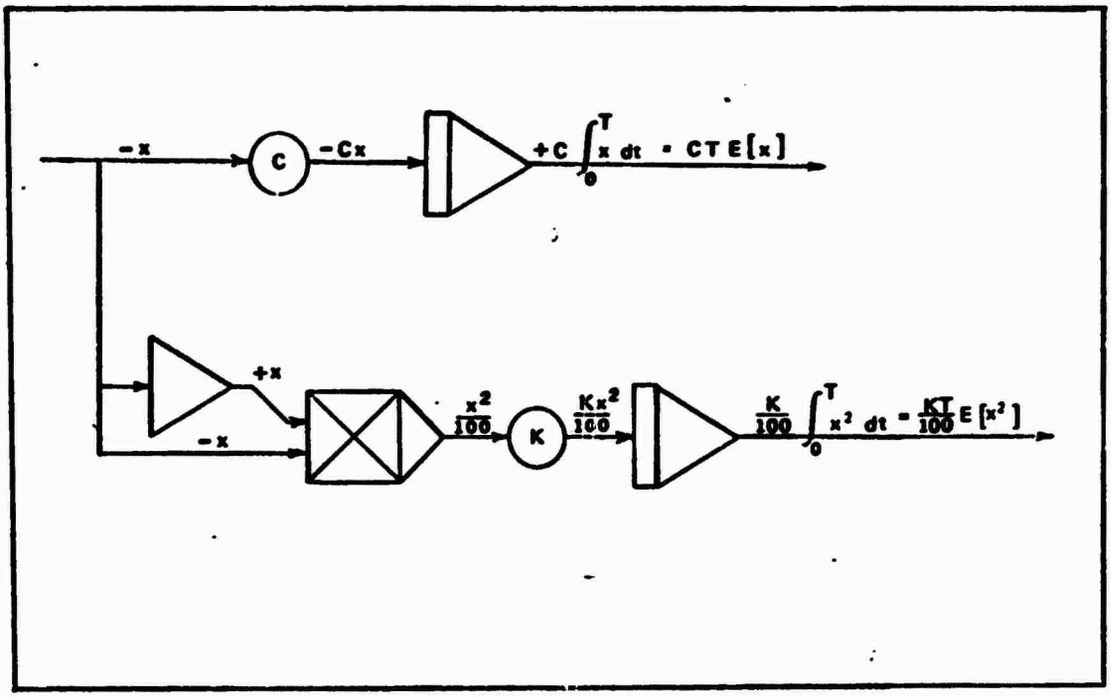

Figure 13. Data Recorder Circuitry

IV. Analytic Solution Using an Optimal Model of the Human Controller

In the past, attempts to model human controller behavior have centered around quasi-linear describing function models consisting of a lag-lead network with remnant (Ref 14). Though these efforts were, for the most part, successful where the task involved compensatory tracking, adaptations of the model to pursuit tracking tasks like the one presented here were not as well received (Ref 15). Work by Kleinman, Baron and Levison has led to the development of a human controller model based upon optimal control theory and the assumption that a "well-trained human operator behaves in an optimal manner subject to his inherent limitations and constraints" (Ref 2:5).

The Kleinman Model

An Overview. Figure 14 is a functional description of the optimal human operator model and its interface with system dynamics. It is assumed that the various sources of human randomness, or remnant, are manifested as errors in perception of displayed variables and in execution of desired control movements. Since the model is linear, these errors are lumped as observation noises, $\underline{v}_y$, and motor noise, v_u, respectively. These v_{y_i} and v_u noises are assumed independent, Gaussian noises of sufficient bandwidth as to be considered white-noise processes with autocovariances

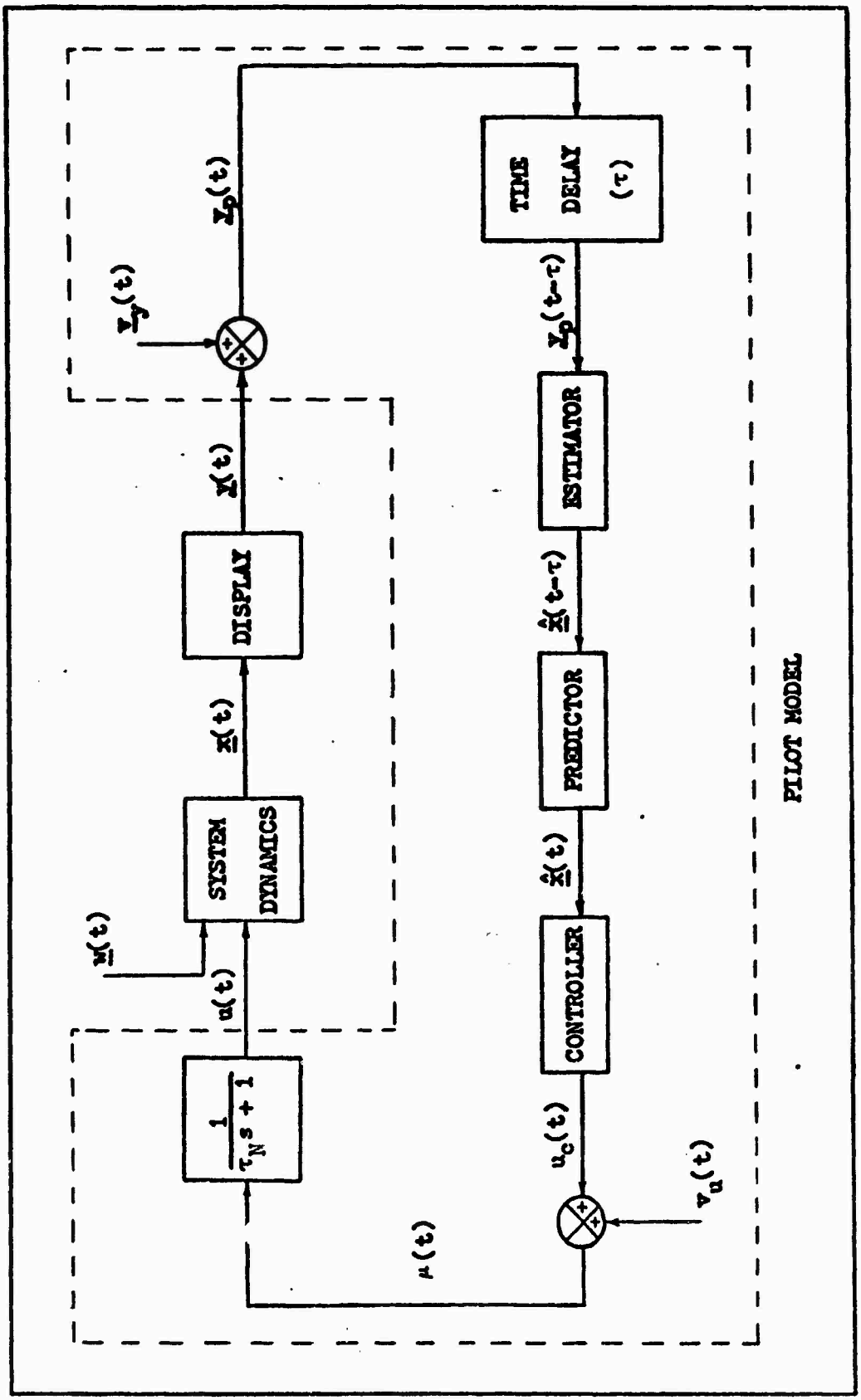

Figure 14. Functional Schematic of the Optimal Pilot Model in the Control Loop.

$$E\{\underline{v}_y(t)\underline{v}_y^T(\tau)\} = V_y\delta(t-\tau) \tag{42}$$

$$E\{v_u(t)v_u(\tau)\} = V_u\delta(t-\tau) \tag{43}$$

The inherent time delays characteristic of human controller behavior, such as perception and reaction delays, are also lumped as an equivalent perceptual time delay, τ. Typical values of τ are 0.2 ± 0.05 seconds (Ref 13:30). This delayed, noisy observation is operated on by a Kalman estimator in cascade with a least mean square predictor to yield a "best estimate", $\hat{\underline{x}}(t)$ of the state at time t, conditioned on the observed output $\underline{y}(\tau), \tau \leq t$. This estimate is then weighted by a set of optimal feedback gains, $-\underline{\ell}^*$, to produce a commanded control input, $u_c(t)$. Note that, for this work, the control input is scalar.

Limitations on the pilot's ability (or willingness) to produce rapid or excessive control movements is accounted for by a first-order lag of the form $(\tau_N s + 1)^{-1}$. In the model, this lag acts upon the noisy commanded control input to produce the actual control input to the system dynamics, u(t). This lag effect creates the need for defining u(t) as the (n+1)th state variable. This gives

$$\tau_N\dot{u}(t) + u(t) = \mu(t) \equiv u_c(t) + v_u(t) \tag{44}$$

or

$$\dot{u}(t) \equiv \dot{x}_{n+1} = -\frac{1}{\tau_N}x_{n+1} + \frac{1}{\tau_N}u_c(t) + \frac{1}{\tau_N}v_u(t) \tag{45}$$

Where $u_c(t)$ is now defined as the control input to the augmented system dynamics.

Creating the Optimal Control. The original system model, assumed linear and time-invariant, is given by

$$\dot{\underline{x}}(t) = A\underline{x}(t) + \underline{b}\, u(t) + \underline{w}(t) \tag{46}$$

$$\underline{y}(t) = H\, \underline{x}\,(t) \tag{47}$$

where $\underline{y}(t)$ is the vector of observed variables and $\underline{w}(t)$ is a zero-mean, Gaussian, white noise vector with covariance

$$W = E\{\underline{w}(t)\underline{w}^T(\tau)\} = W\, \delta(t-\tau) \tag{48}$$

The augmented system is now described by

$$\dot{\underline{z}}(t) = A_1\underline{z}(t) - \underline{b}_1\, u_c(t) + \underline{w}_1(t) \tag{49}$$

where

$$\underline{z}(t) = \text{col}[\underline{x}(t),\, u(t)] \tag{50}$$

$$\underline{w}_1(t) = \text{col}[\underline{w}(t),\, v_u(t)/\tau_N] \tag{51}$$

$$\underline{b}_1 = \text{col}[0,\ldots,0,\, 1/\tau_N] \tag{52}$$

and

$$A_1 = \left[\begin{array}{c|c} A & \underline{b} \\ \hline 0 & -1/\tau_N \end{array}\right] \tag{53}$$

The covariance of $\underline{w}_1(t)$ is now given by

$$E\{\underline{w}_1(t)\underline{w}_1{}^T(\tau)\} = \left[\begin{array}{c|c} W & 0 \\ \hline 0 & V_u/\tau_N{}^2 \end{array}\right] \tag{54}$$

The function of the pilot model is to determine the control input u(t) that minimizes the quadratic cost functional

$$J(u) = \lim_{T\to\infty}\left[\frac{1}{T}E\{\int_0^T(\underline{x}^T Q\underline{x} + ru^2 + g\dot{u}^2)\,dt\}\right]$$

$$= \sum_{i=1}^{n}\sum_{j=1}^{n} q_{ij}\,E\{x_i x_j\} + r\sigma_u^2 + g\sigma_{\dot{u}}^2 \qquad (55)$$

conditioned on the observation $\underline{y}(t)$. In other words, the model is to minimize a weighted combination of the covariances of selected system states and the mean squares of control input and control rate. It can be shown that the optimal control, u(t), is generated by the linear feedback law (Ref 12:360-362).

$$\tau_N\dot{u}(t) + u(t) = u_c(t) + v_u(t) = -\underline{\ell}^*\hat{\underline{x}} + v_1(t) \qquad (56)$$

where

$$\tau_N = 1/\ell_{n+1} \qquad (57)$$

$$\ell^*_i = \tau_N\ell_i, \quad i = 1,2,\ldots,n \qquad (58)$$

$$u_c(t) = -\underline{\ell}^*\hat{\underline{x}} \qquad (59)$$

and the optimal gains, $\underline{\ell}^*$, and the time constant, τ_N, are identical to those that are obtained from the solution of the noise-free regulator problem, i.e., v_u=0 (Ref 2:13). The n+1 feedback gains $\underline{\ell}$ are computed from (Ref 12:360-362).

$$\underline{\ell} = \frac{\underline{b}_o^T K_o}{g} \qquad (60)$$

Where K_o is the unique, positive definite solution to the n+1 dimensional Riccati equation

$$A_o^T K_o + K_o A_o + Q_o - K_o \underline{b}_o \underline{b}_o^T K_o / g = 0 \tag{61}$$

A_o and $\underline{b}_o$ are the augmented matrices

$$A_o = \left[\begin{array}{c|c} A & \underline{b} \\ \hline 0 & 0 \end{array}\right] ; \quad \underline{b}_o = \left[\begin{array}{c} 0 \\ \vdots \\ 0 \\ \hline 1 \end{array}\right] \tag{62}$$

and Q_o is the augmented matrix

$$Q_o = \left[\begin{array}{c|c} Q & 0 \\ \hline 0 & 0 \end{array}\right]$$

The Inner Workings. The pilot is presented a linear combination of the state by means of a display, the output of which is modelled by

$$\underline{y}'(t) = H_1 \underline{z}(t) \tag{63}$$

where H_1 is the constant, augmented observation matrix $H_1=[H:0]$, and $\underline{y}'(t)=\text{col}[\underline{y}(t):0]$. It is assumed that the human operator can perceive not only the state information displayed, but also (and only) the first derivative of that information (Ref 12:359). Due to such remnant effects as random perturbations in human response characteristics, random errors in interpretation of the display, and noisy display systems, the pilot actually perceives a delayed,

noisy rendition of the true system output,

$$\underline{y}'_p(t-\tau) = H_1\underline{z}(t-\tau) + \underline{v}_y(t-\tau) \tag{64}$$

where τ, the equivalent perceptual time delay of the model, defined earlier, was chosen as 0.2 seconds for this study.

From this perceived output, the Kalman filter produces a least mean squared estimate $\hat{\underline{z}}(t-\tau)$ of the delayed state $\underline{z}(t-\tau)$ through the solution to the differential equation (Ref 2:12)

$$\dot{\hat{\underline{z}}}(t-\tau) = [A_1 - CH_1^T V_y^{-1} H_1]\hat{\underline{z}}(t-\tau) + CH_1^T V_y^{-1}\underline{y}'_p(t-\tau) + \underline{b}_1 u_c(t-\tau) \tag{65}$$

where C, the error covariance matrix satisfies, in the steady state (Ref 12:362).

$$A_1C + CA_1^T + W_1 - CH_1^T V_y^{-1} H_1C = 0 \tag{66}$$

The predictor then generates a current-time estimate $\hat{\underline{z}}(t)=\text{col}[\hat{\underline{x}},\hat{u}(t)]$ from

$$\hat{\underline{z}}(t) = e^{A_1^T}[\hat{\underline{z}}(t-\tau) - \underline{\zeta}(t-\tau)] + \underline{\zeta}(t) \tag{67}$$

where

$$\dot{\underline{\zeta}}(t) = A_1\underline{\zeta}(t) + \underline{b}_1 u_c(t) \tag{68}$$

Figure 15 is a detailed diagram of the computational flow involved with this model. Recall that the motor noise present in Figure 14 is now combined with the noise input $\underline{w}_1(t)$ to the system dynamics. Also note that $\underline{\ell}^*_1$ in the diagram as defined at the n+1 dimensional row vector $[\underline{\ell}^*:0]$.

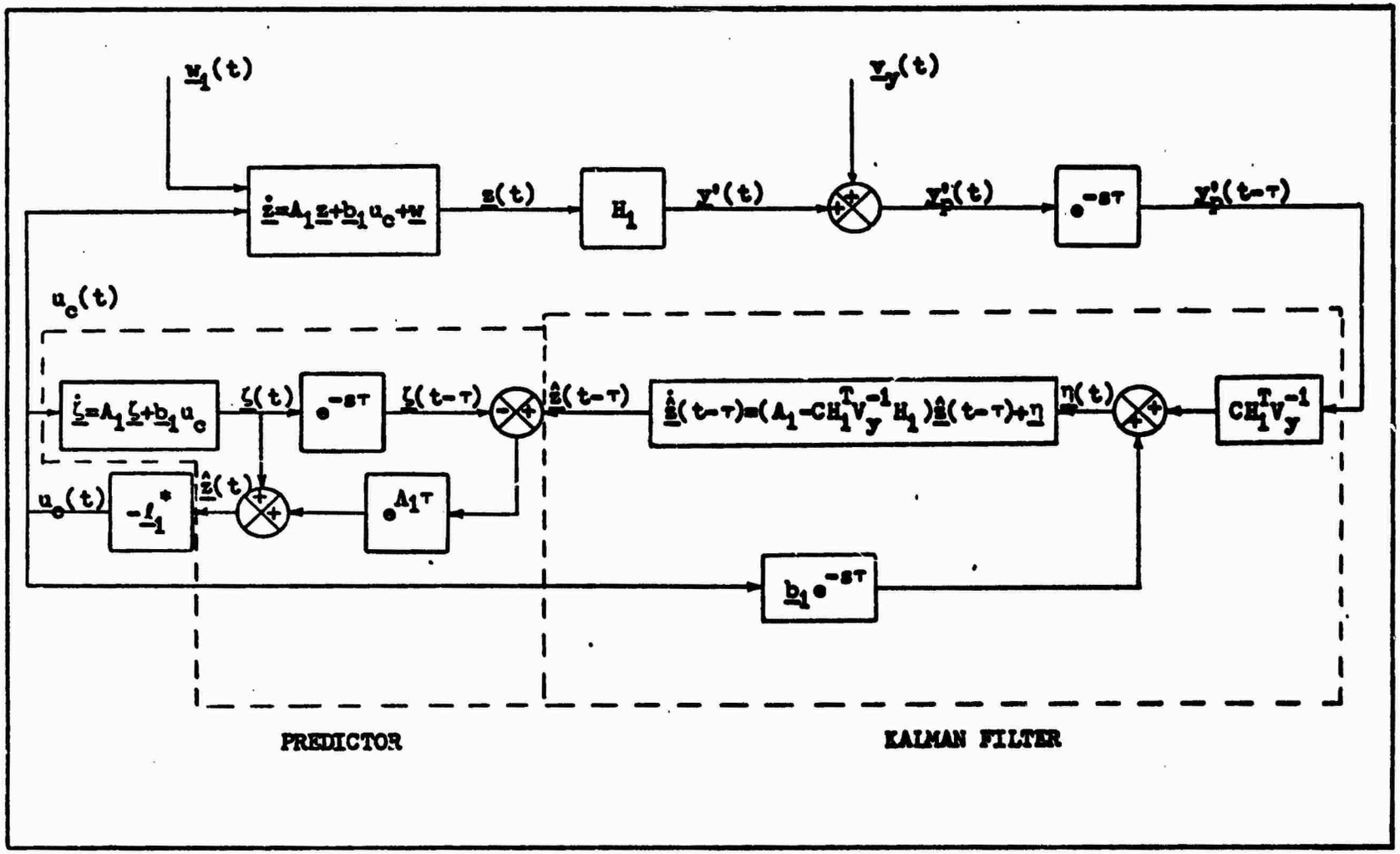

Figure 15. Computational Flow Diagram of the Optimal Pilot Model in the Control Loop (System Equations Augmented).

Finally, the system states statistics are generated in the form of the covariance of $\underline{z}(t)$ through the expression (Ref 12:353)

$$Z = E\{\underline{z}(t)\underline{z}^T(t)\} = e^{A_1\tau} C e^{A_1^T\tau} + \int_o^\tau e^{A_1\sigma} W_1 e^{A_1^T\sigma} d\sigma + \int_o^\infty e^{\bar{A}\sigma} e^{A_1\tau} C H_1^T V_y^{-1} H_1 C e^{A_1^T\tau} e^{\bar{A}\sigma} d\sigma \quad (69)$$

where

$$\bar{A} = \left[\begin{array}{c|c} A & \underline{b} \\ \hline \underline{\ell}^*/\tau_N & -1/\tau_N \end{array}\right] \quad (70)$$

The solution to this equation can be obtained in closed-form by noting that expressions of the form

$$X = \int_o^\infty e^{\bar{A}t} Y e^{\bar{A}^T t} dt \quad (71)$$

can be evaluated from the solution to (Ref 2:143)

$$\bar{A}X = X\bar{A}^T + Y = 0 \quad (72)$$

Further computational methods for the evaluation of (69) are described in Reference 11. The standard deviations, or RMS values, of the system states are then computed as

$$\sigma_{x_i} = \sqrt{Z_{ii}} \quad (73)$$

Application to the Air-to-Air Task

The State Equations of Motion. In the introduction to Section III the dynamic variables describing the air-to-air task were listed. They were repeated here as they were

defined for the state variable format

$$x_1 \equiv \delta$$

$$x_2 \equiv q$$

$$x_3 \equiv \alpha$$

$$x_4 \equiv \lambda$$

$$x_5 \equiv \Sigma_T$$

$$x_6 \equiv \text{dummy state}$$

$$x_7 \equiv A_{n_T}$$

$$x_8 \equiv \gamma_T$$

$$x_9 \equiv \theta$$

Also,

$$u \equiv \delta_c = - K_f F_s$$

Equations (10), (11), (20), (27), (29), (31), and (35) together with the noise filter equations are represented in the system dynamics

$$\dot{\underline{x}}(t) = A\, \underline{x}(t) + \underline{b}\, u(t) + \underline{w}(t) \qquad (74)$$

in which the "A" matrix is

$$
\begin{bmatrix}
\frac{-1}{\tau_a} & 0 & 0 & 0 & 0 & 0 & 0 & 0 & 0 \\
M_\delta + M_{\dot{\alpha}} Z_\delta & M_q + M_{\dot{\alpha}} & M_\alpha + M_{\dot{\alpha}} Z_\alpha & 0 & 0 & 0 & 0 & 0 & 0 \\
Z_\delta & +1 & Z_\alpha & 0 & 0 & 0 & 0 & 0 & 0 \\
0 & +1 & a_{43} & \frac{-1}{T_f} & 0 & 0 & 0 & 0 & 0 \\
0 & 0 & \frac{V_A}{D} & 0 & \frac{V_A - V_T^{\dagger}}{D} & 0 & 0 & \frac{V_T}{D} & \frac{-V_A}{D} \\
0 & 0 & 0 & 0 & 0 & \frac{-1}{\tau_T} & 0 & 0 & 0 \\
0 & 0 & 0 & 0 & 0 & +1 & \frac{-1}{\tau_T} & 0 & 0 \\
0 & 0 & 0 & 0 & 0 & 0 & \frac{-1}{V_T} & -0.01^{*} & 0 \\
0 & +1 & 0 & 0 & 0 & 0 & 0 & 0 & 0
\end{bmatrix}
$$

where

$$a_{43} = \frac{V_A}{V_f}\left(\frac{Z_\alpha}{2} + \frac{J_v}{T_f}\right)$$

Also, $\underline{b} = \text{col}\ [K_L/\tau_a \quad 0 \quad 0 \quad 0 \quad 0 \quad 0 \quad 0 \quad 0 \quad 0]$

and $\underline{w}(t) = \text{col}\ [0 \quad 0 \quad 0 \quad 0 \quad 0 \quad \xi \quad 0 \quad 0 \quad 0\ ]$

where

ξ = white, Gaussian driving noise

---

† This term is zero for all cases studied in this report.

* dummy feedback on this state for stability precautions.

From the display the pilot can extract the computed lead angle, λ, the relative line of sight to the target, Σ_{T_A}, and error, ε, plus the rates of change of each of these quantities. However, Σ_{T_A}, λ, and ε are a linearly dependent set, so that only two of these variables need be represented in the observation vector, $\underline{y}(t)$. The error and line of sight were used along with their respective rates because it was judged that the pilot was more consciously aware of these quantities than the lead angle. Thus the display is modelled by

$$\underline{y}(t) = H\underline{x}(t) \tag{75}$$

with

$$\underline{y}(t) = \begin{bmatrix} \varepsilon \\ \dot{\varepsilon} \\ \Sigma_{T_A} \\ \dot{\Sigma}_{T_A} \end{bmatrix}$$

and H being

$$\begin{bmatrix} 0 & 0 & 0 & +1 & +1 & 0 & 0 & 0 & -1 \\ 0 & 0 & h_{23} & \frac{-1}{T_f} & \frac{V_A-V_T}{D} & 0 & 0 & \frac{V_T}{D} & \frac{-V_A}{D} \\ 0 & 0 & 0 & 0 & -1 & 0 & 0 & 0 & +1 \\ 0 & +1 & \frac{-V_A}{D} & 0 & \frac{V_T-V_A}{D} & 0 & 0 & \frac{-V_T}{D} & \frac{V_A}{D} \end{bmatrix}$$

where

$$h_{23} = \frac{V_A}{D} + \frac{V_A}{V_f}\left(\frac{Z_\alpha}{2} + \frac{J_v}{T_f}\right)$$

Cost Functional Weightings. The weightings on the terms of the cost functional, equation (55), were chosen with the task in mind and after discussions with the pilots who flew the simulation. First, since only fighter aircraft would be involved in this task and failure of the pilot to perform well could have catastrophic results, the weighting on control input, r, was taken to be zero. In this situation, the pilot's control inputs would only be limited by the "G" loadings he could physically withstand. Of course, theoretically he could withstand an infinite number of "G's" in this fixed-base simulation.

When performing air-to-air tracking, the pilot is aware primarily of the tracking error and the rate of change of that error. Both are kept to a minimum by the pilot; the former for obvious reasons, and the latter because excessive rates lead to overshoots and pilot-induced oscillations (PIO) that lead to even greater error. Further, the emphasis on low tracking error rate is a consequence of the "smoothness" of his flying technique that is inbred in a pilot from his first flying lesson. Therefore, it was decided to weight the error and its rate equally in the cost functional. Since error is not a system state, but is a linear combination of states [see equation (37)] in the system output equation, a weighting matrix Q' in $\underline{y}^T Q' \underline{y}$ where

$$Q' = \begin{bmatrix} 1 & 0 & 0 & 0 \\ 0 & 1 & 0 & 0 \\ 0 & 0 & 0 & 0 \\ 0 & 0 & 0 & 0 \end{bmatrix} \qquad (76)$$

would yield the same effect as Q in $\underline{x}^T Q \underline{x}$ when $Q \equiv H^T Q' H$.

Finally, the weighting on control rate, g, is specified when the neuro-motor lag time constant, τ_N, is specified. This is due to the relationship between τ_N and l_{n+1} given by equation (57) and the fact that the solution to the Riccati equation (61) relies upon a knowledge of g. Emperical data have shown that τ_N is of the order of 0.1 to 0.6 seconds, with $\tau_N \simeq 0.1$ seconds being typical (Ref 12:363). Consequently the 0.1 value was used in this study.

Determination of the Noise Covariances. Since the observation and motor noises depend upon the quality of the display, distractions related to the environment, and human randomness, determination of numerical values for their covariances, V_y, and V_u, respectively, can be quite difficult. However, it has been found that each white observation noise $v_{y_i}(t)$ has a covariance that is related to the variance of its associated variable y_i by (Ref 12:363)

$$V_{y_i} = \pi \rho_i E\{y_i^2\} \tag{77}$$

where, on the average, ρ_i=0.01, which was used herein.

Similarly, the motor noise covariance is assumed to be related to the variance of the commanded control, $u_c(t)$, by (Ref 12:363)

$$V_u = \pi \rho_u E\{u_c^2\} \tag{78}$$

Data-matching methods described in Reference 12 yield a typical valve for ρ_u of 0.003 which was also utilized in this study.

The state equations for the target motion noise filters

$$\dot{x}_6 = -\frac{1}{\tau_T} x_6 + \xi \tag{79}$$

$$\dot{x}_7 = x_6 - \frac{1}{\tau_T} x_7 \tag{80}$$

or

$$\dot{\underline{x}}' = A'x' + \underline{w}'(t) \tag{81}$$

where

$$A' = \begin{bmatrix} -\frac{1}{\tau_T} & 0 \\ 1 & -\frac{1}{\tau_T} \end{bmatrix} ; \quad \underline{x}' = \begin{bmatrix} x_6 \\ x_7 \end{bmatrix} \tag{82}$$

and

$$\underline{w}'(t) = \begin{bmatrix} w_6(t) \\ w_7(t) \end{bmatrix} = \begin{bmatrix} \xi \\ 0 \end{bmatrix} \tag{83}$$

Note that the "primes" indicate submatrices, not the transpose.

The covariance of $\underline{w}'(t)$ is

$$W' = E\{\underline{w}'(t)\underline{w}'^{T}(t)\} = \begin{bmatrix} E\{\xi^2\} & 0 \\ 0 & 0 \end{bmatrix} \tag{84}$$

The evaluation of W' is made from (Ref 11:1-6)

$$A'X' + X'A'^{T} + W' = 0 \tag{85}$$

where X' is the symmetric covariance matrix of $\underline{x}'(t)$

$$X = E\{\underline{x}'(t)\ \underline{x}'^{T}(t)\}$$

$$= \begin{bmatrix} X_{66} & X_{67} \\ X_{76} & X_{77} \end{bmatrix} \tag{86}$$

and

$$X_{66} = \sigma^2_{x_6} \equiv \text{variance of } x_6(t)$$

$$X_{77} = \sigma^2_{x_7} \equiv \text{variance of } x_7(t)$$

$$X_{76} = X_{67} = E\{x_6(t)x_7(t)\}$$

Since the variance of x_7 is just the square of the RMS target accelerations stipulated in the simulation, equation (85) can now be evaluated to obtain

$$W' = \begin{bmatrix} w_{66} & 0 \\ 0 & 0 \end{bmatrix} \tag{87}$$

where

$$w_{66} = \frac{4\sigma^2_{A_{n_T}}}{\tau_T^3}$$

Now, x_6 is the only state affected directly by $\underline{w}(t)$, so W, the covariance of $\underline{w}(t)$ is null except for element w_{66}.

Modelling Threshold Effects

In any visual task there exists a limit on the minimum arc of resolution that the controller can physically perceive. This is known as the visual threshold. Also, there usually exists a minimum error signal to which a human may not respond.

This is known as the indifference threshold. The former threshold can be qualitatively evaluated through data-matching; however the latter would have a high dependency on the situation involved. For instance, a pilot may not be too concerned with a certain glide path deviation at five miles from touchdown in the landing approach, whereas that same deviation may be totally unacceptable at one mile range.

In the pilot model for this task these effects are not distinguished and are modelled as a statistical linearization of the "deadzone" nonlinearity shown in Figure 16 where (Ref 9:87-95)

$$f(y) = \begin{cases} y - a, & y \geq a \\ 0, & -a < y < a \\ y + a, & y \leq -a \end{cases} \qquad (88)$$

This amounts to replacing this nonlinearity with an equivalent gain $\hat{f}(y)$. This gain, always less than unity, is plotted versus $a_x/(\sqrt{2}\ \sigma_x)$ in Figure 16, as taken from Ref. 6, page 238. Here the parameter "a" is the actual minimum deviation that can be resolved by the observer. It has been found that 0.05° is the typical minimum arc of resolution (Ref 9:93). Since in this simulation 20 inches separated the observer from the display, this 0.05° converts to approximately 0.05cm on the oscilloscope. To accomodate the large lead angles generated at the 3000-foot range, it was necessary to scale the display to approximately 13° per cm. Therefore, the error threshold, a_ε, for this simulation was computed to be 0.65°. Typical values for rate threshold are ~0.05 to

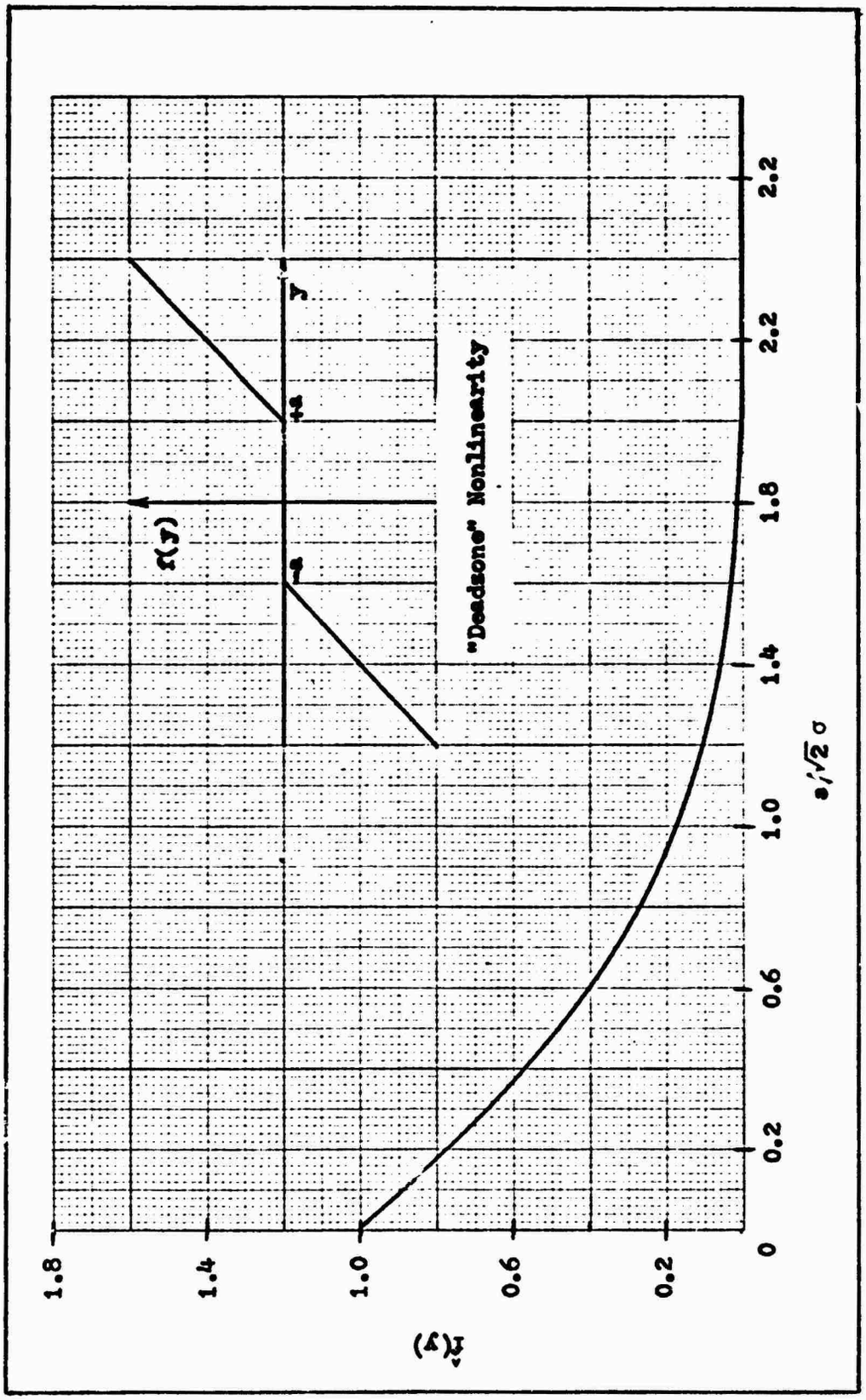

Figure 16. Threshold Nonlinearity and Equivalent Gain Plot

0.10 degrees of visual arc per second (Ref 8:15). Using the upper limit in this simulation, the error rate threshold, $a_{\epsilon}^{\cdot}$, was computed to be 1.3 degrees per second.

Thus the image presented to the pilot appears as

$$y_{p_i}(t) = \hat{f}_i(y) y_i(t) + v_{y_i}(t) \tag{89}$$

or

$$y^*_{p_i}(t) = y_i(t) + \hat{f}_i^{-1}(y)\, v_{y_i}(t) \tag{90}$$

Therefore, when the effects of threshold are taken into account, the covariance of each observation noise is given by

$$V_{y_i} = \pi \rho_i f_i^{-2}(y)\, E\{y_i^2\} \tag{91}$$

The Pilot Model in Action

The objective of this chapter has been to present the equations and rationale of the Kleinman pilot model applied to the air-to-air tracking task. In practice, the computations are performed by means of a digital computer program. The program used in this study was adapted from that presented in Reference 13 by Major James D. Dillow, Assistant Professor of Mathematics at the Air Force Institute of Technology, Wright-Patterson Air Force Base, Ohio. A brief description of that program follows.

After the situational data, e. g., stability derivatives, velocities, altitudes, target noise covariance, etc., and cost functional weightings are input to the program, the feedback gains, $\underline{\ell}$, and consequently τ_N, are computed. If the desired value of τ_N is not achieved, the weighting on the control

rate, g, is adjusted and the computations repeated. This process is repeated until the proper weighting has been discovered that yields the desired τ_N. The optimal feedback gains are now known.

The uncorrelated observation and motor noises are now added to the system in the form of initial guesses at the values of their respective covariance matrices V_y and V_u. Enough information is now known to compute the error covariance, C, from equation (66). The covariances of the system states, which, in the augmented form, include the control, u(t), are then computed from equation (69). Finally, new values for V_y and V_u are calculated using equations (91) and (78), respectively. If the differences between the new and old values of the noise covariances are not tolerable, the process is repeated until convergence on the correct, within tolerances, covariances is achieved. The RMS values of the pilot model performance indexes are then computed from equation (73).

The results obtained from the pilot model "flying" all twelve test cases is compared in the next section with those obtained from the analog simulation.

V. Analysis of Results

Table II and Figures 17 through 21 are a summary of the preliminary findings of this study. There is very definitely a one-to-one correlation between predicted and actual elevator deflection, lead angle, and line of sight. However, it would appear at first glance that the pitch rate and error plots do not correlate very well--a very serious flaw, since the ability to track with minimum error is a prime consideration when judging the effectiveness of a weapon system in this task. A second look is more revealing. Look first at pitch rate. In every case, the computer generated more pitch rate than did the pilots in the simulation. However, there is a marked distinction between pitch rate magnitudes at the 3000-foot range and those at 1000 feet. For clarity, a line has been drawn separating the two groups on the plot.

Now look at the plot of tracking error. Though the data points are somewhat scattered, in the mean there does appear to be almost a one-to-one correlation between predicted and actual error at the 1000-foot range, the correlation becoming better as the target motion reduces from 5.0G to 3.5G. The 3000-foot data is another story. A line drawn through the mean of this grouping has a slope of almost one-half, meaning that the computer is tracking nearly twice as well as the simulation pilots.

The pitch rate and error grouping tendency led to a deeper analysis of the differences in dynamics at the two

Table II. Comparison of RMS Performance Data, Equal Weighting on Error and Error Rate

Case	Elevator (δ) (Degrees)		Pitch Rate (q) (Degrees/Sec)		Lead Angle (λ) (Degrees)		LOS (ΣT_A) (Degrees)		Error (ε) (Degrees)	
	Analog	Digital	Analog	Digital	Analog	Digital	Analog	Digital	Analog	Digital
F-4E/3000'/3.5G	1.755	1.889	6.395	9.384	8.721	9.000	8.855	8.571	2.355	1.300
F-5/3000'/3.5G	1.083	1.309	6.130	11.09	11.14	11.72	10.55	11.22	2.778	1.407
A-7/3000'/3.5G	3.573	4.074	7.730	10.67	9.888	10.75	10.21	10.38	2.487	1.373
F-4E/3000'/5.0G	2.420	2.637	9.221	12.61	12.06	12.64	12.46	12.15	2.671	1.535
F-5/3000'/5.0G	1.512	1.751	9.094	14.33	15.76	16.43	14.21	15.89	3.666	1.605
A-7/3000'/5.0G	5.276	5.756	11.03	14.80	14.21	15.26	14.06	14.83	2.841	1.676
F-4E/1000'/3.5G	2.136	2.152	8.022	9.223	2.866	2.874	2.732	2.486	2.136	2.413
F-5/1000'/3.5G	1.313	1.233	7.462	8.415	3.006	2.982	2.542	2.550	2.059	1.895
A-7/1000'/3.5G	4.920	5.022	11.24	12.22	3.895	3.873	3.975	3.464	2.664	2.811
F-4E/1000'/5.0G	2.980	3.065	11.20	13.03	3.970	4.072	3.684	3.512	2.746	3.273
F-5/1000'/5.0G	1.780	1.751	10.69	11.87	4.303	4.231	3.899	3.627	2.836	2.507
A-7/1000'/5.0G	7.111	7.158	15.58	17.36	5.464	5.511	5.428	4.928	3.519	3.889

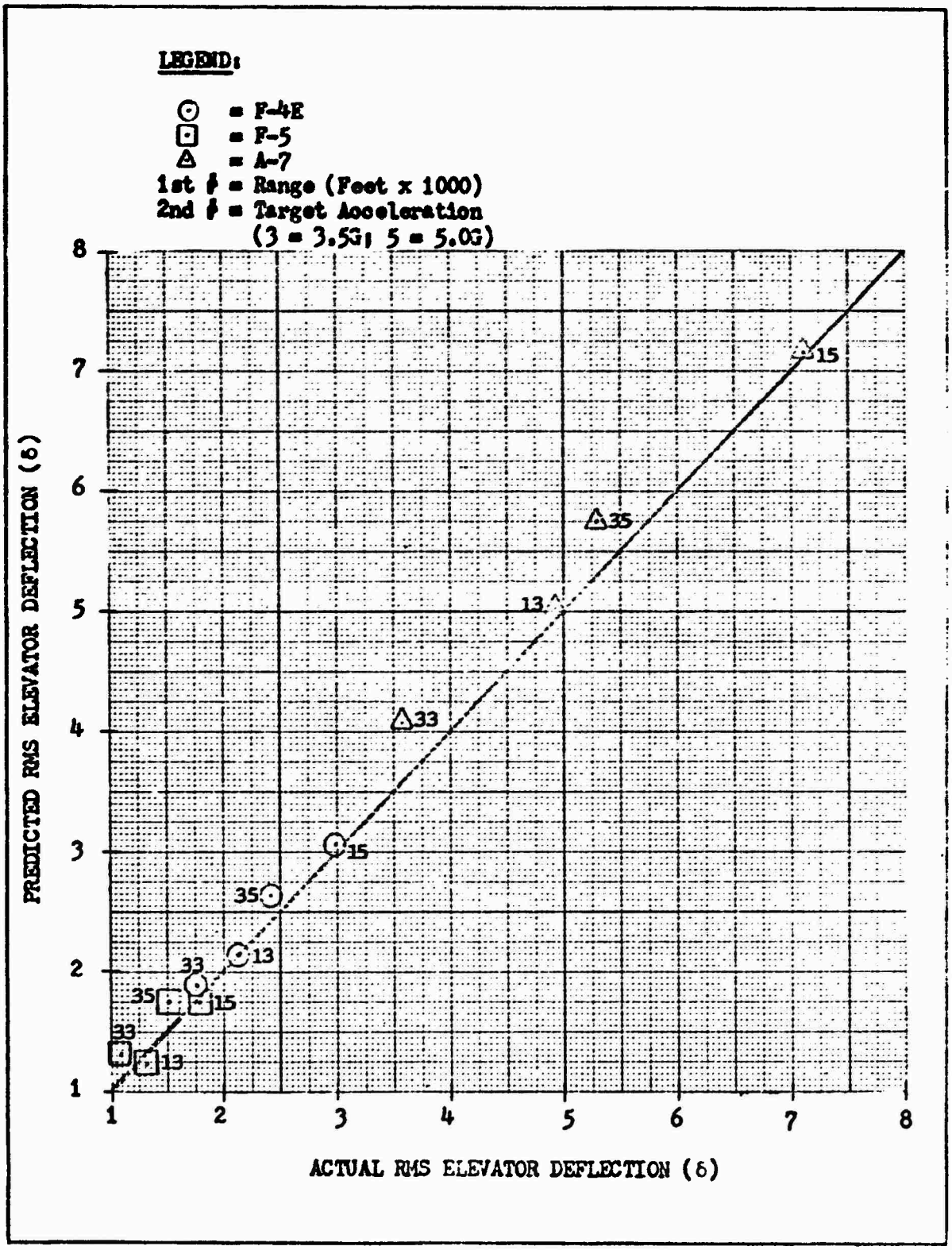

Figure 17. Predicted Versus Actual RMS Elevator Deflection (Degrees). Equal Weighting on Error and Error Rate.

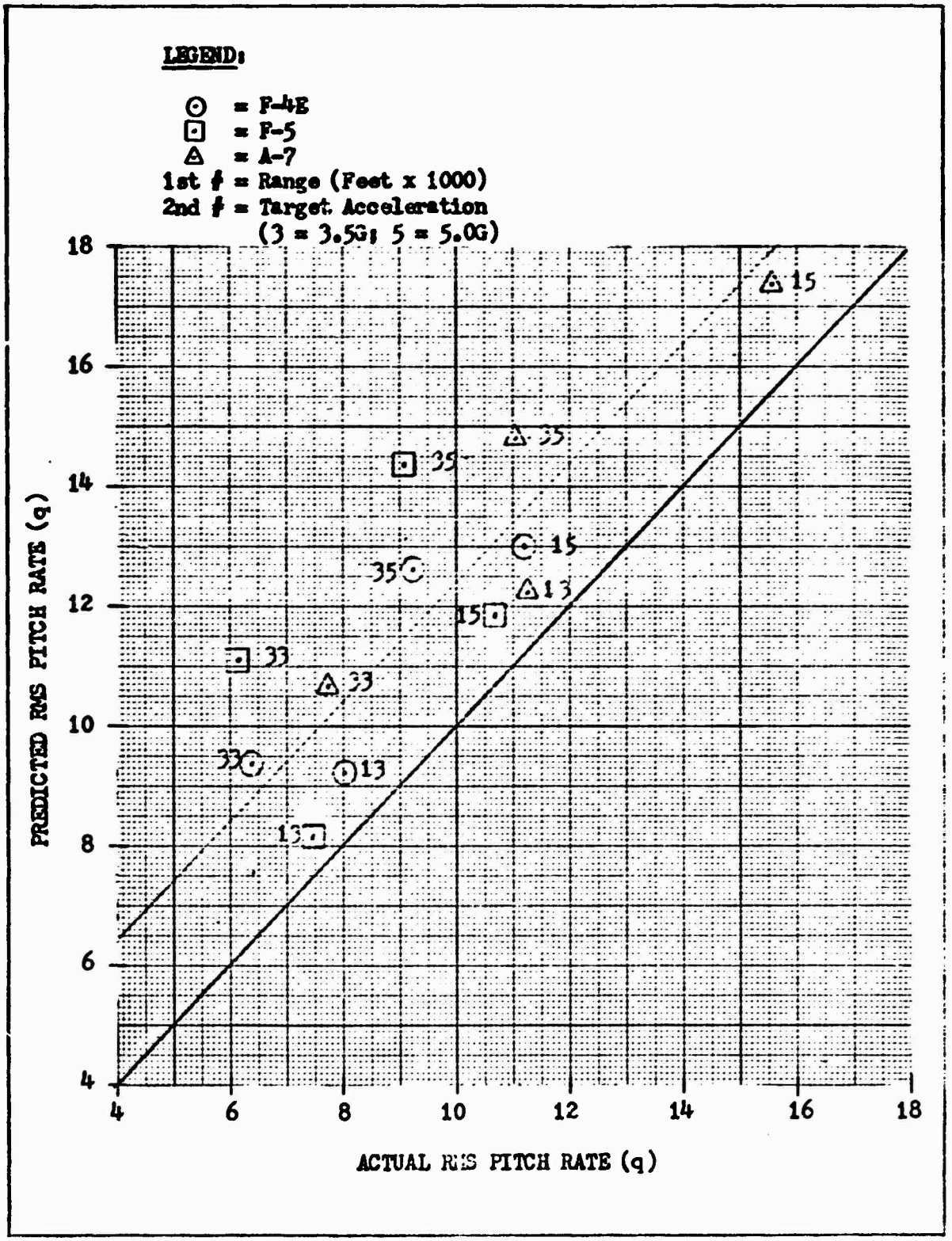

Figure 18. Predicted Versus Actual RMS Pitch Rate (Degrees/Second). Equal Weighting on Error and Error Rate.

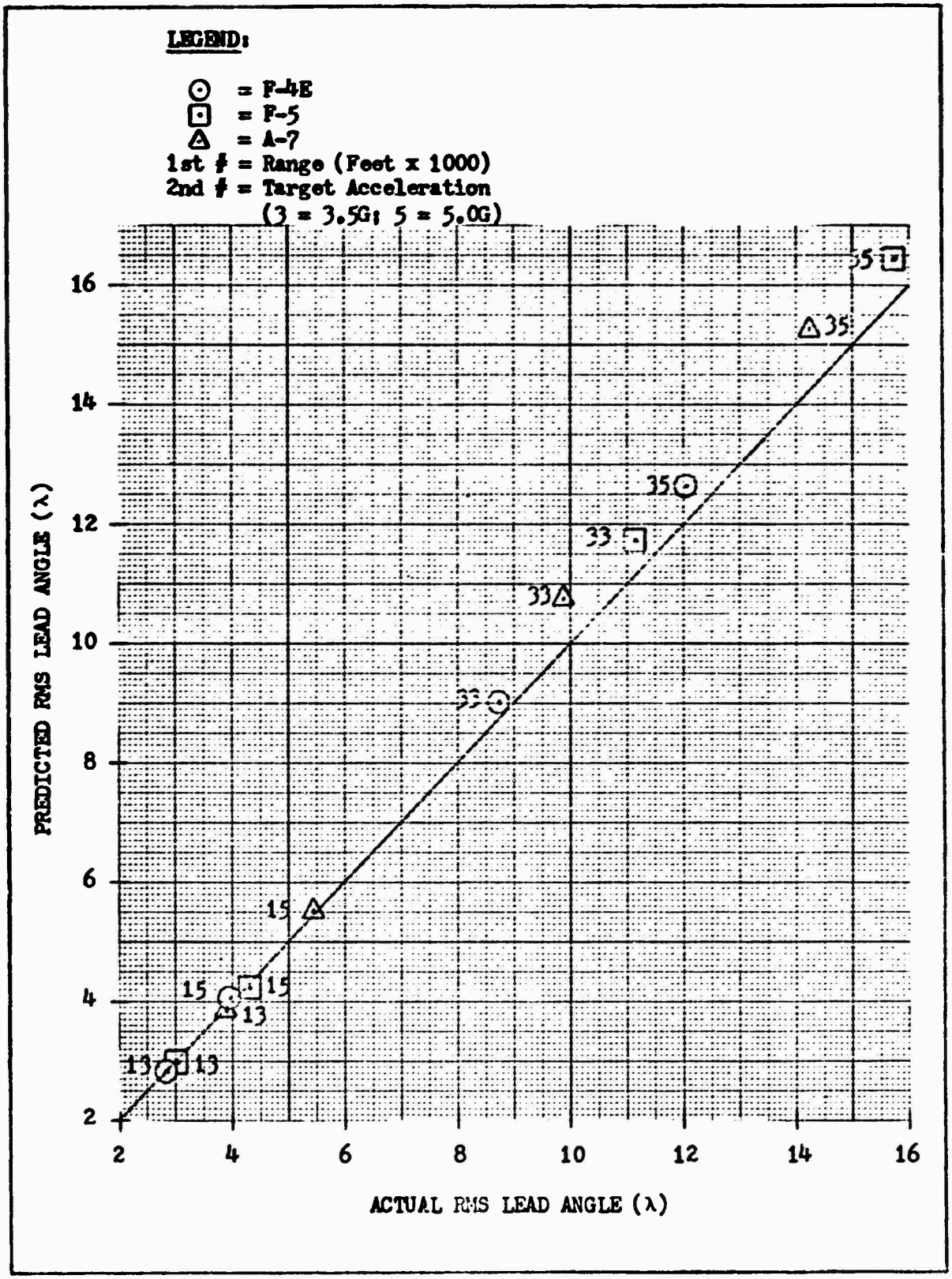

Figure 19. Predicted Versus Actual RMS Lead Angle (Degrees). Equal Weighting on Error and Error Rate.

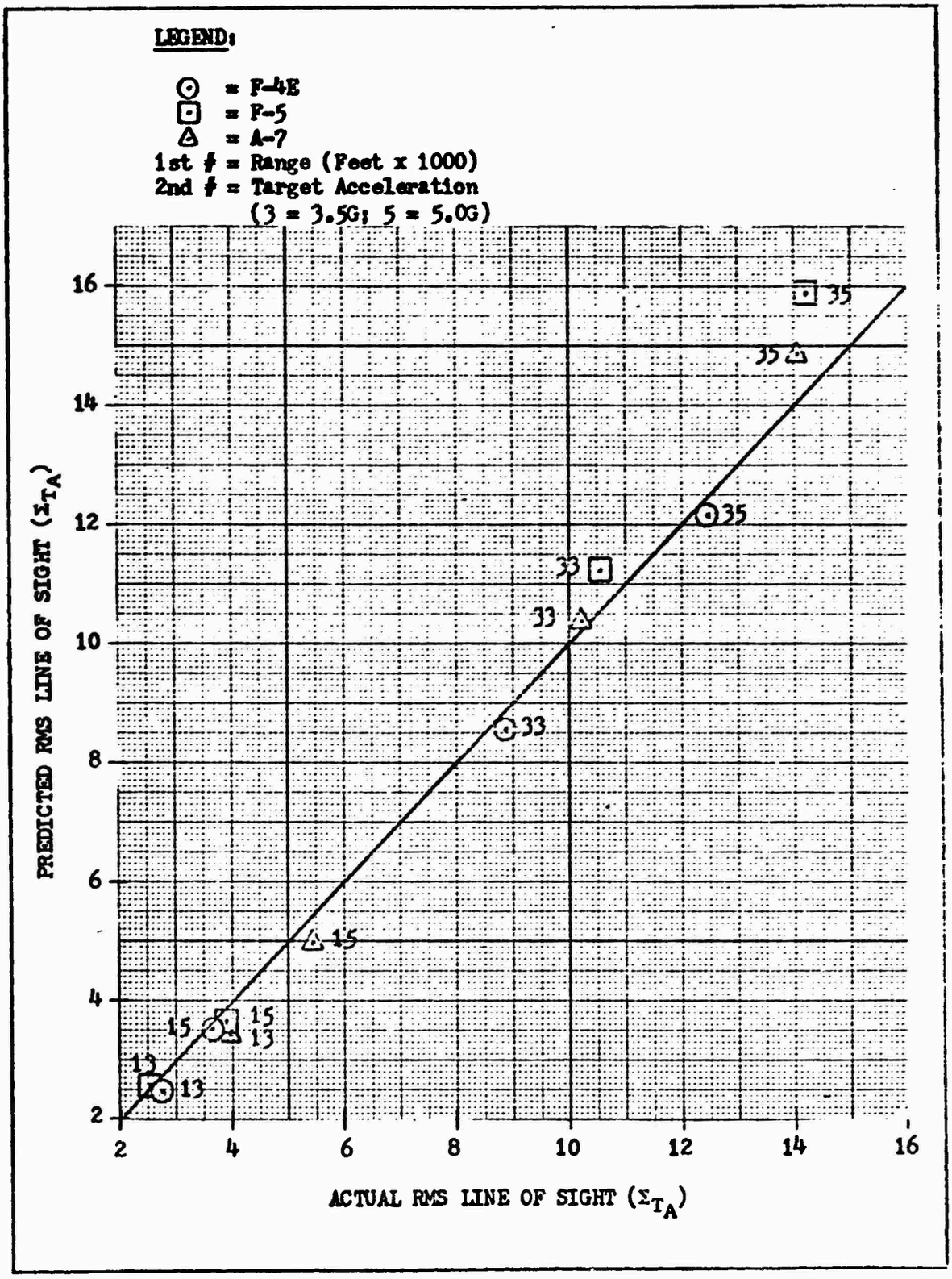

Figure 20. Predicted Versus Actual RMS Line Of Sight (Degrees). Equal Weighting on Error and Error Rate.

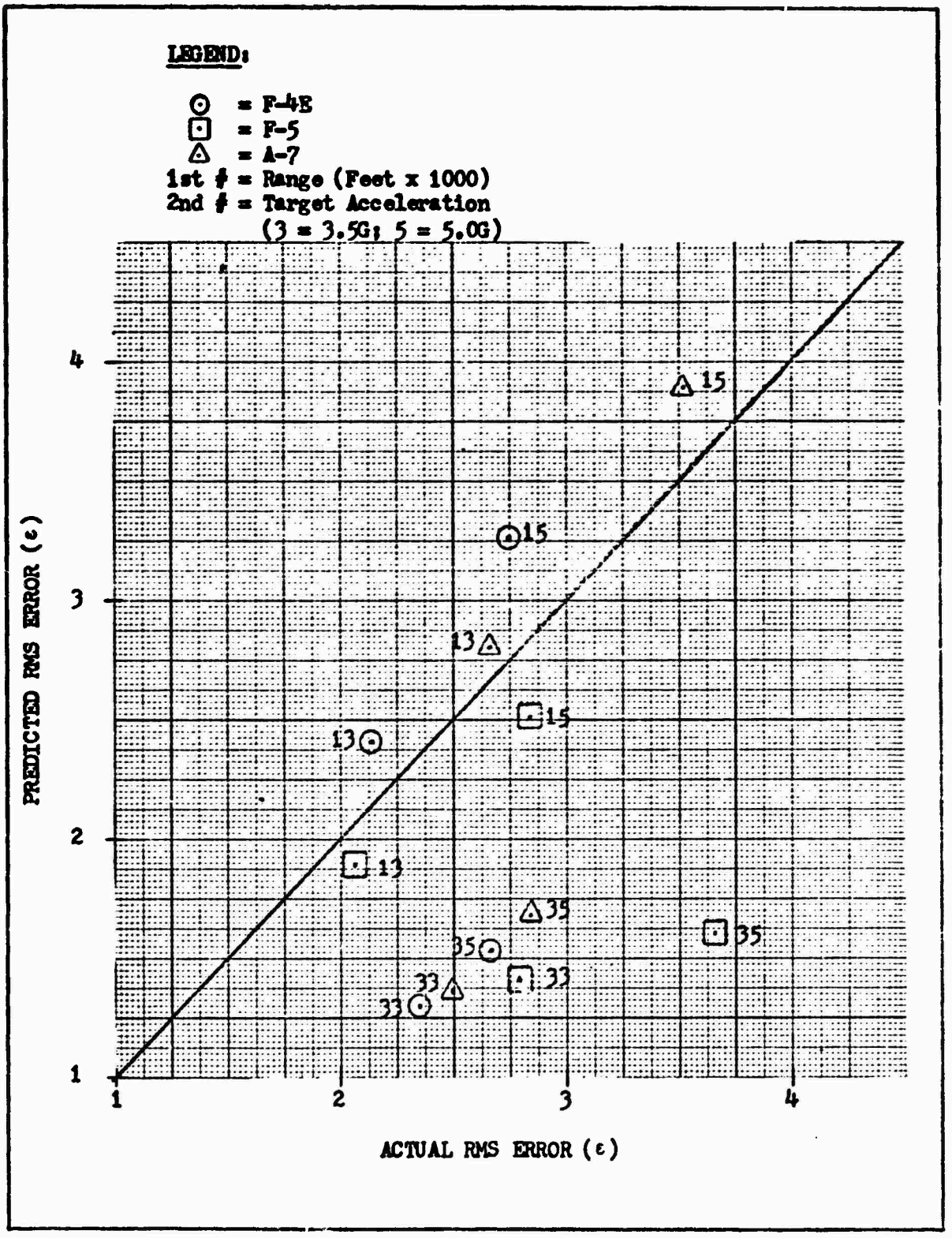

Figure 21. Predicted Versus Actual RMS Error (Degrees). Equal Weighting on Error and Error Rate.

ranges. The answer was found in the sight equation, (20). As was stated in Section II, in practice the sight parameters T_f and V_f are normally held constant at some nominal value determined from nominal conditions of altitude, temperature, velocities, and range. However, in this study the sight time constant, T_f, the projectile time of flight, and V_f, the projectile average relative velocity, were recomputed for each case by the method shown in Appendix A. In effect, then, changing ranges changed the sight, just as if the "black boxes" in the aircraft had been changed! The difference is amazing. At 1000 feet, T_f averaged 0.34 seconds. This compares with 1.38 seconds at 3000 feet--a factor of four. Thus, in addition to the generation of larger lead angles, the sight dynamics were accentuated in the form of more visible oscillations. The pilots found that they could not be as aggressive at this range because of the sight sensitivity. Large pitch rates generated large sight overshoots, and the resulting long settling time deprived the pilot of the exact knowledge of his tracking error. So the pilots compensated. They reduced their pitch rate and concentrated on "easing" the sight onto the target. This, of course, led to longer periods in which the sight was not on the target and, consequently, greater RMS tracking error than would have been expected.

So, through subjective questioning of other fighter pilots it was decided that relative weightings of $\varepsilon = 3$, $\dot{\varepsilon} = 1$, and $\dot{\lambda} = 2$ might work. Since the cost functional is

quadratic, Q′ becomes

$$Q' = \begin{bmatrix} 9 & 0 & 0 & 0 \\ 0 & 5 & 0 & 4 \\ 0 & 0 & 0 & 0 \\ 0 & 4 & 0 & 4 \end{bmatrix} \qquad (92)$$

With these weightings, the results tabulated in Table III were obtained. Plots of predicted versus actual parameters are presented in Figures 21 through 26. Only slight improvement can be seen in δ, λ, and Σ_{T_A}. However, marked improvement can be seen in both pitch rate and tracking error. The added weighting on sight rate and the reduced weighting on error rate has had the effect of considerably increasing the tracking error at 3000 feet while having a smaller detrimental effect on the 1000-foot errors. The data points are still far from a perfect match, but they are quite acceptable. More work needs to be done toward finding the rationale for computing an optimum set of weightings.

The results not only correlate quite well, but they also make good intuitive sense. Note that for a given range and target motion the data point out the relative strengths of the different aircraft in performing this task. For instance, at the 1000-foot range the F-5 was predicted to be the best aircraft for the task (per "G" level), followed closely in ability by the F-4E, and then by the A-7. With one slight anomaly at the 5G level, the simulation data indicates likewise. Since the F-5 is primarily an air-to-air fighter, the F-4E more multi-

Table III. Comparison of RMS Performance Data, Additional Weighting on Lead Angle Rate

Case	Elevator (δ) (Degrees)		Pitch Rate (q) (Degrees/Sec)		Lead Angle (λ) (Degrees)		LOS (Σ_{T_A}) (Degrees)		Error (ε) (Degrees)	
	Analog	Digital	Analog	Digital	Analog	Digital	Analog	Digital	Analog	Digital
F-4E/3000'/3.5G	1.755	1.821	6.395	7.402	8.721	9.125	8.855	8.280	2.355	2.232
F-5/3000'/3.5G	1.083	1.052	6.130	7.119	11.14	11.78	10.55	10.80	2.778	2.431
A-7/3000'/3.5G	3.573	3.968	7.730	9.314	9.888	10.87	10.21	10.21	2.487	2.270
F-4E/3000'/5.0G	2.420	2.570	9.221	10.30	12.06	12.82	12.46	11.80	2.671	2.776
F-5/3000'/5.0G	1.512	1.474	9.094	9.867	15.76	16.55	14.21	15.40	3.666	2.942
A-7/3000'/5.0G	5.276	5.629	11.03	13.11	14.21	15.44	14.06	14.61	2.841	2.918
F-4E/1000'/3.5G	2.136	2.148	8.022	9.241	2.866	2.947	2.732	2.774	2.136	2.682
F-5/1000'/3.5G	1.313	1.221	7.462	8.341	3.006	3.023	2.542	2.745	2.059	2.163
A-7/1000'/3.5G	4.920	4.990	11.24	12.25	3.895	3.949	3.975	3.823	5.428	5.426
F-4E/1000'/5.0G	2.980	3.059	11.20	13.08	3.970	4.181	3.684	3.919	2.746	3.705
F-5/1000'/5.0G	1.780	1.736	10.69	11.79	4.303	4.289	3.899	3.885	2.836	2.906
A-7/1000'/5.0G	7.111	7.114	15.58	17.41	5.464	5.618	5.428	5.426	3.519	4.374

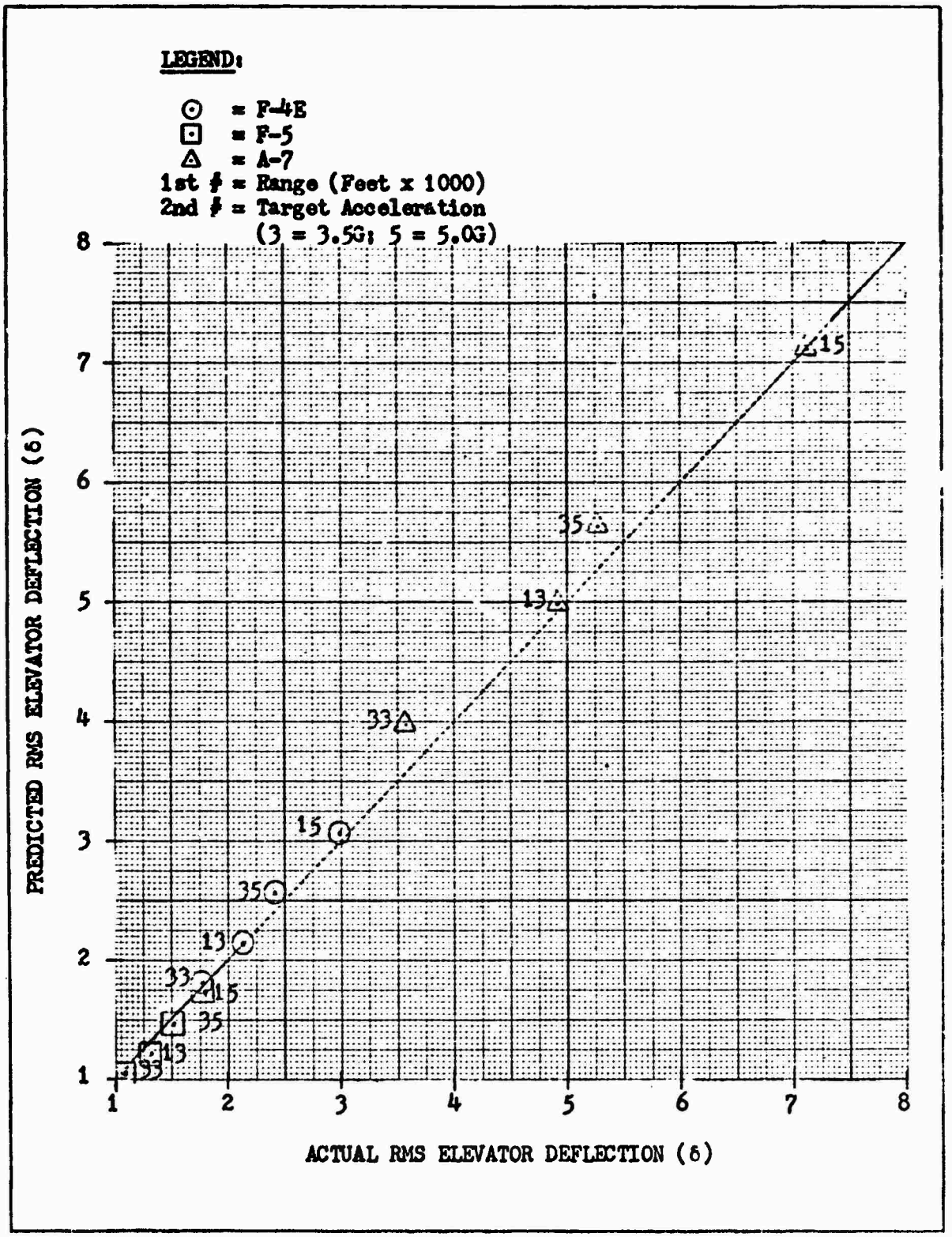

Figure 22. Predicted Versus Actual RMS Elevator Deflection (Degrees). Additional Weighting on Lead Angle Rate.

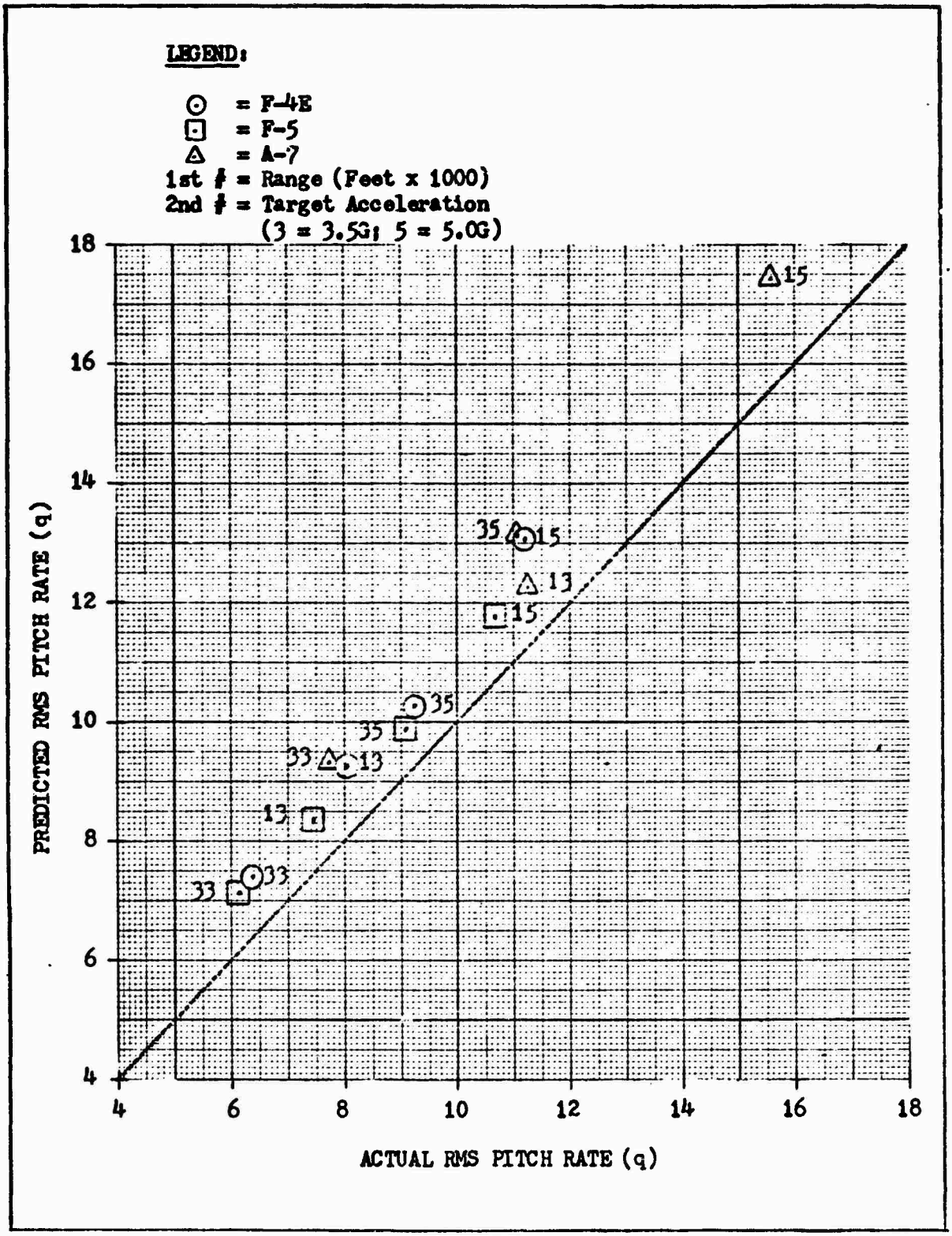

Figure 23. Predicted Versus Actual RMS Pitch Rate (Degrees/Second). Additional Weighting on Lead Angle Rate.

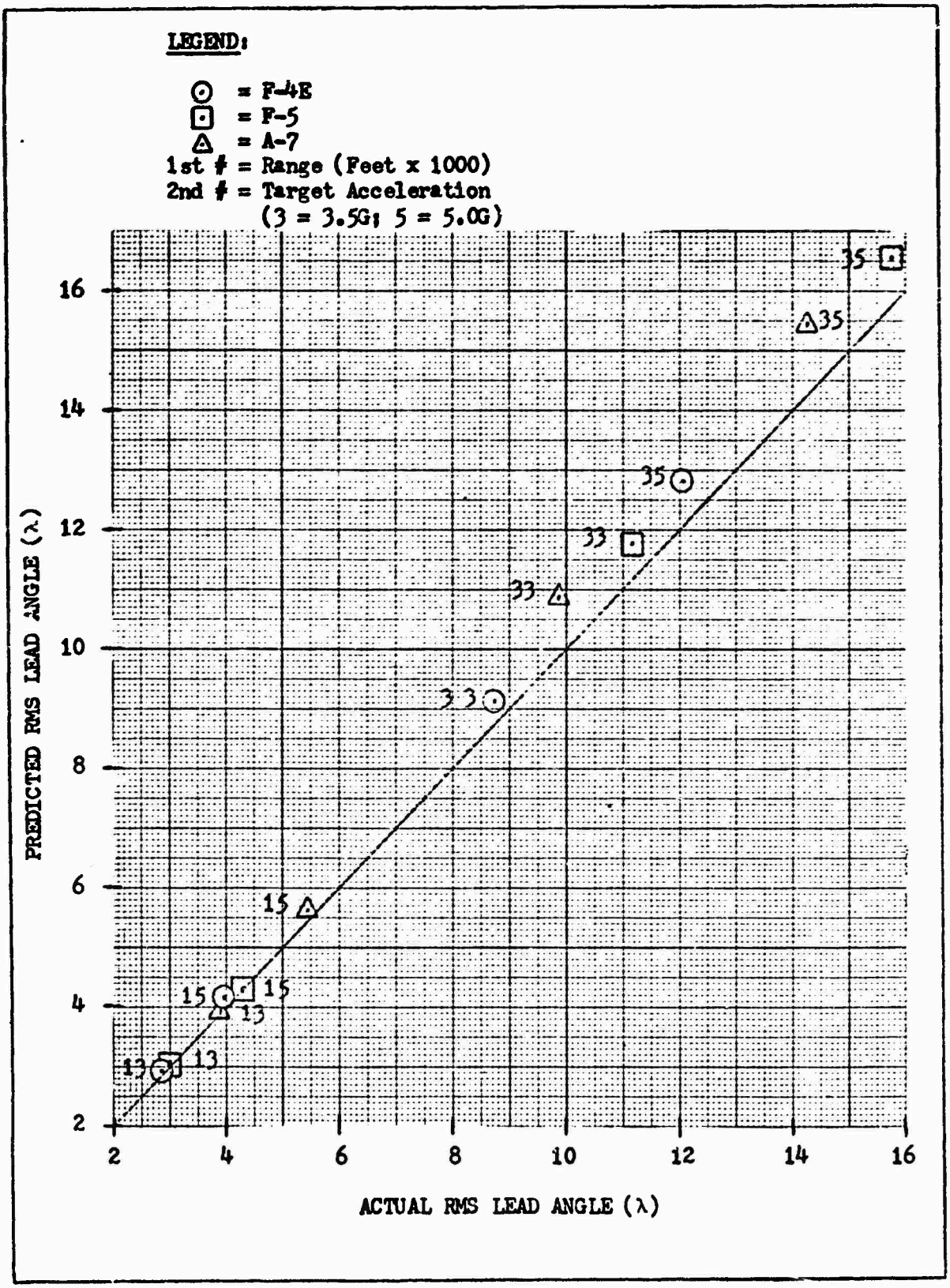

Figure 24. Predicted Versus Actual RMS Lead Angle (Degrees). Additional Weighting on Lead Angle Rate.

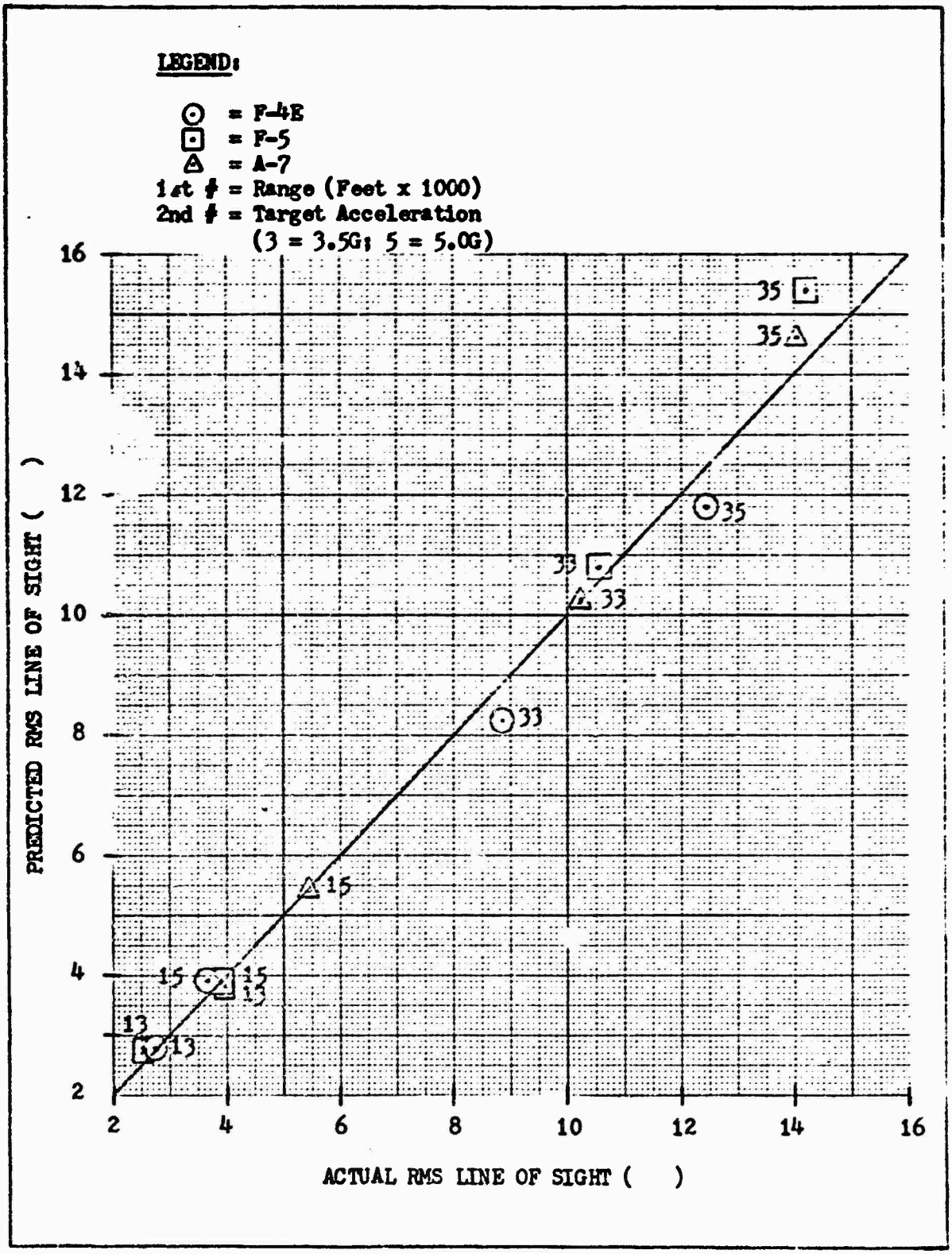

Figure 25. Predicted Versus Actual RMS Line Of Sight (Degrees). Additional Weighting on Lead Angle Rate.

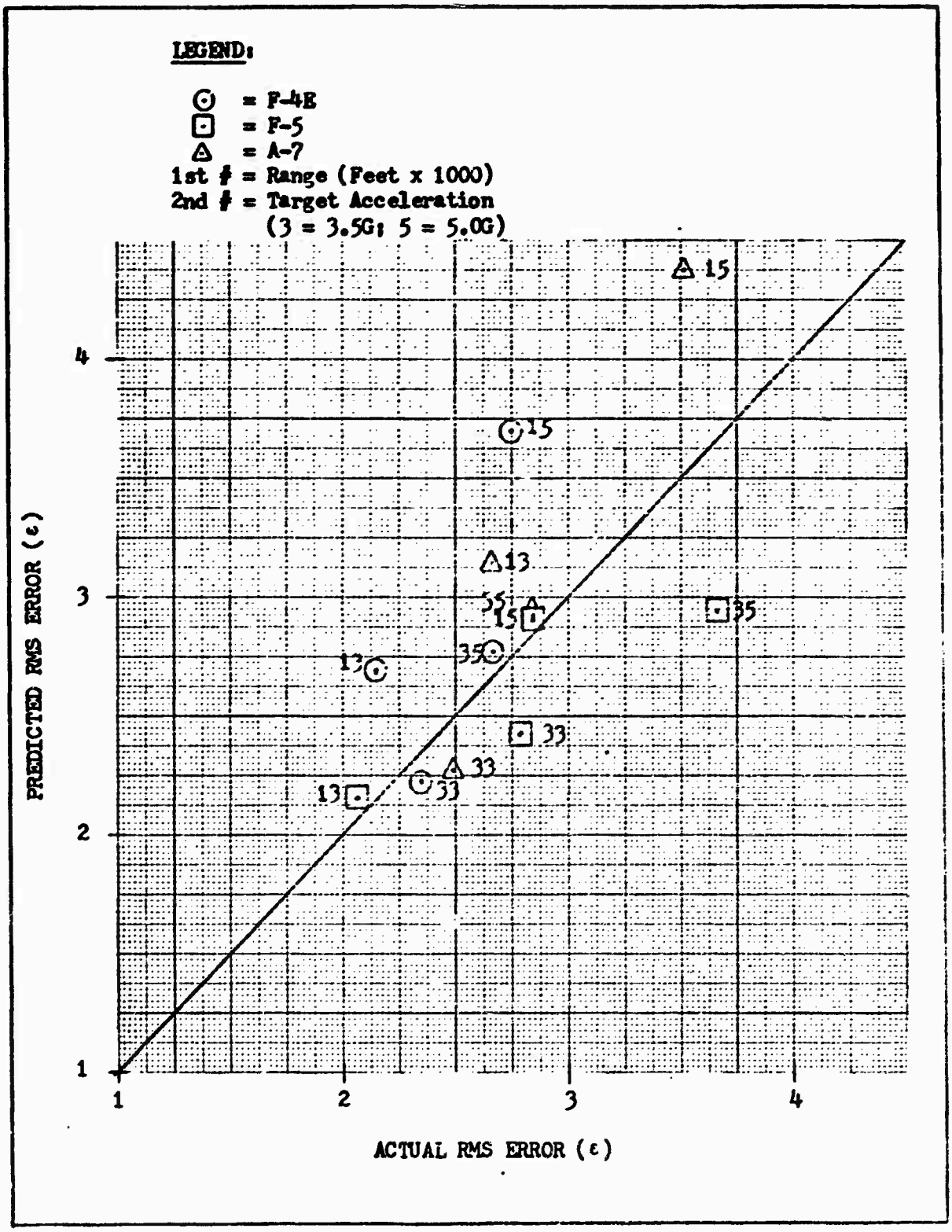

Figure 26. Predicted Versus Actual RMS Error (Degrees). Additional Weighting on Load Angle Rate.

purpose in design, and the A-7 primarily an air-to-ground weapon, the results make sense. On the other hand, at the 3000-foot range the F-4E is judged the best, followed by the A-7. Last is the F-5. The principal reason for this is the extremely responsive nature of the longitudinal dynamics of the F-5. It is so pitch sensitive that it aggrevates the problems with the sight dynamics at this long range. On the other hand, the A-7 is very sluggish (comparatively speaking) in the longitudinal axis, a feature that was very helpful in damping the sight oscillations at this range.

It should be noted that the relative performance figures given here are not strictly indicative of one aircraft's ability to perform relative to another. The situational parameters chosen for this work were done with an attempt in mind toward obtaining a good "spread" in the data. The F-5 at 5.135 feet and 0.81 Mach represents a good, responsive environment; the A-7 at 15,000 feet and 0.61 Mach represents a sluggish set of parameters, by comparison; and finally, the F-4E at 15,000 feet and 0.9 Mach would be classified as a good median situation. This analysis is born out by the groupings of data points on elevator deflection in Figures 17 and 22. When these groupings are compared with the resulting pitch rate statistics in Figures 18 and 23, it can be seen that the F-4E required somewhat more elevator travel than the F-5 to produce roughly the same amount of pitch rate. The

difference is even more pronounced with the A-7. The higher pitch rates generated with the A-7 are a consequence of the response lag produced by its sluggish environment. By the time the aircraft responded, tracking error was greater and higher rates were required to reduce that error.

Another look at the elevator deflection plots indicates that, regardless of the level of performance achieved in any one situation, the pilots certainly had to work much harder with the A-7 than with the F-5 or F-4E. This conclusion was substantiated by the pilots themselves.

A final note before concluding: there should be no attempt made to correlate aircraft tracking performance differences between the two ranges used. Since sight dynamics were changed each time range was changed, one would be comparing an aircraft having a sight designed for 3000 feet and being used at 3000 feet against one having a sight designed for 1000 feet and being used at that range. Obviously, with given, constant sight parameters, tracking error would almost always be less at the 3000-foot range than at 1000 feet.

VI. Concluding Remarks and Recommendations

Conclusions

The "scatter diagrams" of Section V speak for themselves. In fact, when applied to the results of this study, the term "scatter" is almost a misnomer. One can but conclude that, given the ideal simulation conditions used in this study (two-dimensional, linear, stationary, Gaussian, zero-mean), the model of the human controller exhibited herein is a superb imitation of a human pilot when performing the air-to-air tracking task with an LCOS system. It would appear that one need only give judicious thought toward evaluation of the proper weightings, Q', on the displayed variables and toward consideration of the threshold effects of the display available in order to be able to predict the performance of given aircraft, flight control, and sight combinations.

The only weak link in the model seems to lie in the selection of these weightings on state. They are, of course, critical to the success of the predictions derived from the execution of the pilot model. The predicted magnitudes of lead angle, elevator deflection, and line of sight were found to be fairly insensitive to changes in the weightings. However, pitch rate and error were very sensitive to these changes and, since tracking error is the prime factor in the evaluation of system performance, great care must be taken in the selection of these weightings. They must therefore reflect intimate knowledge of human controller behavior in the environment created for him by the task

at hand.

An alternative to rigorous selection of relative state weightings would be to use such weightings as are given in this report and use the pilot model to obtain performance data on a system of known performance quality. Then other systems could be analyzed based upon performance relative to this base system.

Recommendations

The success of this study should open the door to expanded study of the application of this pilot model to other tasks, such as air-to-ground weapon delivery. For the present, however, there is much continuation work needed in the application of the model to the air-to-air task. The next step should be to perform a time-varying simulation which would account for closure of the attacker on the target. This would require extension of the pilot model to the time-varying case. The results of this study should then be compared with the results published herein to determine if the simpler, stationary model is not adequate for evaluation of system performance.

Of course, three-dimensional modelling and testing of the pilot model in the air-to-air environment is definitely warranted. No study is complete until this has been done. The lateral and yaw dynamics thus added would require formulation of a pilot model capable of multiple control outputs.

Further extension of the model to include nonlinearities

such as varying velocities and velocity jump should then follow. Once again, the pilot model would have to be modified to accept a nonlinear plant.

Another possibility would be the development of a model for the error propagation for the bullet as a function of the attacker states and target motion so as to compute the probability of a kill.

Finally, contingent upon the outcome of this later research, industry should seriously consider the potential of this model for providing inexpensive, much-needed testing of integrated subsystems at the "idea" level. This testing would reveal any serious deficiencies in required performance characteristics before the actual hardware is built. In fact, this approach could be used to synthesize an "optimal" integrated fire control/flight control system in a relatively inexpensive manner.

Bibliography

1. Anderson, R. O., and J. D. Dillow. "Paper Pilot" -- An Application of Pilot Models to Predict VTOL Flying Qualities in Precision Hover. Proceedings of the Sixth Annual Conference on Manual Control: pp 349-364. Wright-Patterson Air Force Base, Ohio: April, 1970.

2. Baron, S., et al. Application of Optimal Control Theory to the Prediction of Human Performance in a Complex Task. AFFDL-TR-69-81. Wright-Patterson Air Force Base, Ohio: Air Force Flight Dynamics Laboratory, March, 1970.

3. Biezad, D. L. A Method of Predicting Pilot Rating for the Pitch Handling Qualities of Aircraft Flown on the Glide Slope. AFIT Thesis GA/MA/73-1. Wright-Patterson Air Force Base, Ohio: Air Force Institute of Technology, December, 1973.

4. Blakelock, John H. Automatic Control of Aircraft and Missiles. New York: John Wiley and Sons, Inc., 1965.

5. General Electric Company. Air-To-Air Gunnery Improvement For F-4E Per FSCP-34. ACD 9986. Binghamton, New York: General Electric Company, Avionic Controls Department, August 15, 1970.

6. Graham, Dunstan, and Duane McRuer. Analysis of Nonlinear Control Systems. New York: Dover Publications, Inc., 1971.

7. Hackford, R. H. Analysis of Piloted Weapon Delivery: F-4E Aerial Gunnery. AFIT Thesis GGC/EE/72-3. Wright-Patterson Air Force Base, Ohio: Air Force Institute of Technology, June, 1972.

8. Kleinman, D. L., and S. Baron. A Control Theoretic Model for Piloted Approach to Landing. Unpublished paper. Cambridge, Massachusetts: Bolt Beranek and Newman Inc.

9. Kleinman, D. L., and S. Baron. Analytic Evaluation of Display Requirements for Approach to Landing. NASA CR-1952. Washington: National Aeronautics and Space Administration, November, 1971.

10. Kleinman, D. L. and T. Perkins. "Modelling the Human in a Time-Varying Anti-Aircraft Tracking Loop." Submitted for publication in IEEE Transactions on Automatic Control, May 1973.

11. Kleinman, D. L. An Iterative Technique for Riccati Equation Computations. BBN Technical Memorandum DLK-1. Cambridge, Massachusetts: Bolt Beranek and Newman Inc., June 30, 1970.

12. Kleinman, D. L., S. Baron, and W. H. Levison. "An Optimal Control Model of Human Response, Part 1," Automatica, 6:357-363 (May 1970).

13. Levison, W. H., and D. L. Kleinman. Analysis of Pilot/System Performance in Carrier Approach. Cambridge, Massachusetts: Bolt Beranek and Newman Inc., September, 1971.

14. McRuer, D. T. and H. R. Jex. "A Review of Quasi-Linear Pilot Models." IEEE Transactions on Human Factors in Electronics, HFE-8:231-249 (September 1967).

15. McRuer, et al. New Approaches to Human Pilot/Vehicle Dynamic Analysis. AFFDL-TR-67-150. Wright-Patterson Air Force Base, Ohio: Air Force Flight Dynamics Laboratory, February, 1968.

16. Meditch, J. S. Stochastic Optimal Linear Estimation and Control. New York: McGraw-Hill Book Company, 1969.

17. Onstott, E. D., E. P. Salmon, and R. L. McCormick. Prediction and Evaluation of Flying Qualities in Turbulence. AFFDL-TR-71-162. Wright-Patterson Air Force Base, Ohio: Air Force Flight Dynamics Laboratory, February, 1972.

18. Quinlivan, R. P. Multimode Flight Control Definition Study For Precision Weapon Delivery. AFFDL-TR-71-39. Wright-Patterson Air Force Base, Ohio: Air Force Flight Dynamics Laboratory, June, 1971.

19. Rankine, R. R., Jr., The Effects of Aircraft Dynamics and Pilot Performance on Tactical Weapon Delivery Accuracy. Doctoral Dissertation. Los Angeles, California: University of California at Los Angeles, 1970.

20. Wrigley, W., and J. Hovorka. Fire Control Principles. New York: McGraw-Hill Book Company, Inc., 1959.

21. Bryan, Ralph S. Unpublished report on ballistics modelling. AFAL/NVE-1. Wright-Patterson Air Force Base, Ohio: Air Force Avionics Laboratory, July 12, 1973.

Appendix A

Determination of Projectile Time of Flight And Average Relative Velocity

Equation (20), used to compute the required lead angle, λ, is dependent upon two projectile trajectory parameters, the values of which are not altogether readily apparent. They are T_f, the time of flight of the projectile to impact with the target, and V_f, the average velocity of the projectile relative to the weapon station over this time of flight. Both parameters are, of course, dependent upon each other as well as target range, velocity, and maneuvering tactics. This addendum relates the simple manner in which "ball park" estimates of these two parameters were computed. Perfection was not the goal, so, with respect to some of the assumptions made, realism was sacrificed somewhat in favor of simplicity.

For the purposes of this study, nominal values for T_f and V_f were computed based upon the tracking ranges, altitudes, and airspeeds to be used in the simulation. The target was limited to constant 3.5 G and 5.0 G turns. It was assumed that the tracking aircraft had achieved the proper lead angle and that projectile impact on the target would occur after T_f seconds of flight. Figure 27 shows the geometry involved.

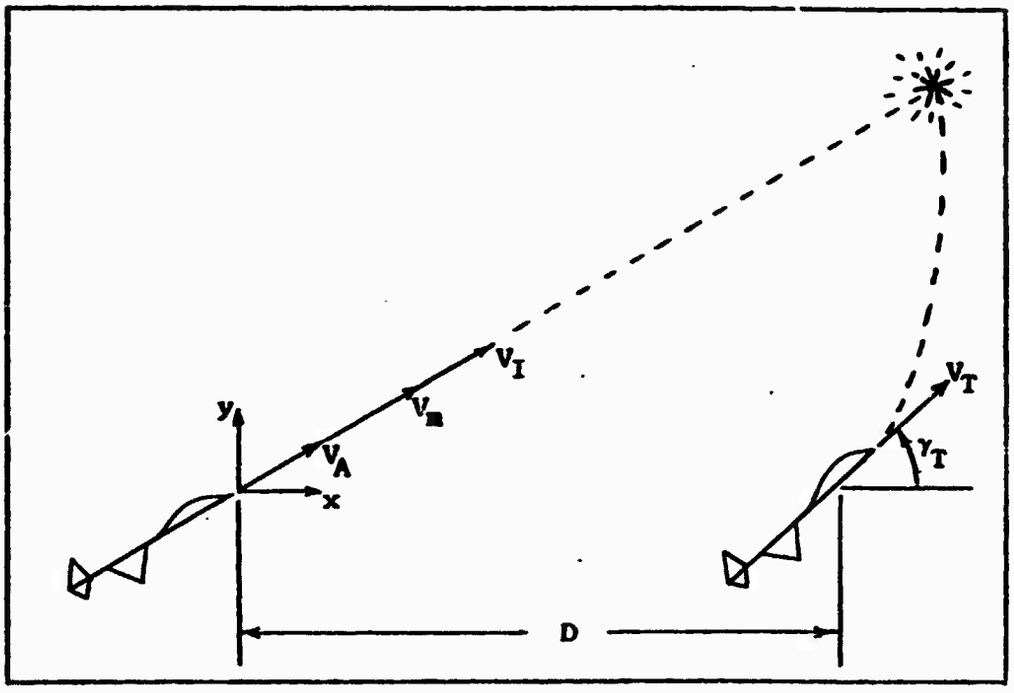

Figure 27. Projectile Trajectory Geometry

The attacker angle of attack was assumed zero so that

$$|\underline{V}_I| = |\underline{V}_A + \underline{V}_m| = |\underline{V}_A| + |\underline{V}_m| \tag{93}$$

where

V_I = initial projectile total velocity

V_m = projectile muzzle velocity

V_A = attacking aircraft velocity

Current techniques in ballistics modelling use the integral of

$$\dot{V}_p = - 2K_B \left(\frac{\rho}{\rho_o}\right) V_p^{3/2} \tag{94}$$

to calculate projectile velocity, V_p, at any time, t, after firing. Here ρ is the atmospheric density at the flight altitude, ρ_o is sea level atmospheric density, and K_B is a ballistic constant producing best correspondence with appropriate ballistic tables (Ref 21:3). K_B was chosen as 0.00614 in this study from an analysis of ballistics tables F-7 and F-8 on page F-16 of Reference 5.

The range of the target from the position the attacker occupied at the time of firing is given by

$$\underline{R}_T = \begin{bmatrix} R_{T_x} \\ R_{T_y} \end{bmatrix} \tag{95}$$

So, from the geometry given in Figure 27, the velocity of the target can be modelled by

$$\underline{V}_T = \begin{bmatrix} V_{T_x} \\ V_{T_y} \end{bmatrix} = \begin{bmatrix} \dot{R}_{T_x} \\ \dot{R}_{T_y} \end{bmatrix} = \begin{bmatrix} V_T \cos \gamma_T \\ V_T \sin \gamma_T \end{bmatrix} \tag{96}$$

As was pointed out in Section III, γ_T can be computed from the solution to

$$\dot{\gamma}_T = - \frac{1}{V_T} A_{n_T} \tag{35}$$

Finally, the time rate of change of projectile position, $\underline{R}_p$, is

$$\dot{\underline{R}}_p = \underline{V}_p = \begin{bmatrix} \dot{R}_{p_x} \\ \dot{R}_{p_y} \end{bmatrix} \tag{97}$$

So, equations (35), (94), (96), and (97) were integrated in a digital computer program using a Runge-Kutta integration routine. At each step, the range of the projectile, $|\underline{R}_p|$, and the range of the target, given by

$$|\underline{R}_T| = \sqrt{R_{T_x}^2 + R_{T_y}^2} \tag{98}$$

were compared to determine if impact had occurred. When impact occurred, the elapsed time in the Runge-Kutta routine was then T_f. The average velocity of the projectile was then

$$V_{avg} = \frac{1}{T_f} \int_o^{T_f} V_p \, dt \tag{99}$$

It can be shown that (Ref 7:66)

$$V_p = V_I \, e^{-K_B \rho R_p} \tag{100}$$

Therefore,

$$V_{avg} = \frac{V_I}{T_f} \int_o^{T_f} e^{-K_B \rho R_p} \, dt \tag{101}$$

$$= \frac{V_I}{K_B \rho R_p} \left(1 - e^{-K_B \rho R_p}\right) \tag{102}$$

The average relative velocity of the projectile, V_f, after T_f seconds of flight was then

$$V_f = V_{avg} - V_A \tag{103}$$

Appendix B

Tabulated Simulation Data

Table IV.

Simulation Data:

Range - 3000 Feet

Target RMS Acceleration - 3.5 G

Type A/C	Pilot Number	Elevator (δ) (Degrees)		Pitch Rate (q) (Degrees/Sec)		Lead Angle (λ) (Degrees)		LOS (Σ_{T_A}) (Degrees)		Error (ε) (Degrees)	
		Mean	RMS	Mean	RMS	Mean	RMS	Mean	RMS	Mean	RMS
F-4E	1	+0.145	1.727	-0.476	6.400	-0.760	8.658	-0.990	8.931	+0.240	2.265
	2	+0.056	1.814	-0.199	6.807	-0.252	8.856	-0.341	9.165	+0.093	2.171
	3	+0.038	1.725	-0.113	5.978	-0.156	8.649	-0.817	8.469	+0.659	2.629
F-5	1	-0.016	1.175	+0.092	5.868	+0.238	10.92	+0.156	9.288	+0.080	2.441
	2	+0.107	1.078	-0.643	7.042	-0.311	11.42	-1.282	11.59	+0.020	2.594
	3	+0.082	0.988	-0.518	5.479	-0.883	11.07	-0.990	10.78	+0.105	3.299
A-7	1	-0.226	3.625	+0.478	7.837	+0.674	10.04	-0.035	10.59	+0.718	2.631
	2	+0.097	3.572	-0.203	8.127	-0.244	9.867	+0.221	10.21	-0.461	2.361
	3	+0.114	3.521	-0.232	7.225	-0.290	9.751	-1.107	9.830	+0.830	2.469

Table V.

Simulation Data:

Range - 3000 Feet

Target RMS Acceleration - 5.0 G

Type A/C	Pilot Number	Elevator (δ) (Degrees)		Pitch Rate (q) (Degrees/Sec)		Lead Angle (λ) (Degrees)		LOS (Σ_{T_A}) (Degrees)		Error (ε) (Degrees)	
		Mean	RMS	Mean	RMS	Mean	RMS	Mean	RMS	Mean	RMS
F-4E	1	+0.032	2.417	-0.110	8.899	-0.159	12.11	-0.280	12.54	+0.129	3.030
	2	+0.080	2.439	-0.312	9.776	-0.370	11.99	-0.493	12.62	+0.124	2.287
	3	+0.085	2.403	-0.258	8.986	-0.418	12.10	-0.845	12.22	+0.431	2.696
F-5	1	-0.054	1.531	+0.672	8.807	+0.731	15.74	+0.806	13.31	-0.075	3.772
	2	-0.052	1.473	+0.954	9.799	+0.748	15.73	+0.920	15.9?	-0.180	3.229
	3	+0.002	1.533	+0.023	8.676	-0.102	15.81	-0.138	13.38	+0.037	3.997
A-7	1	+0.090	5.162	-0.199	11.12	-2.340	14.18	-0.169	12.53	-0.063.	2.713
	2	-0.050	5.102	+0.126	11.56	+0.162	14.10	-0.200	15.13	+0.362	2.789
	3	+0.226	5.563	-0.494	10.42	-0.512	14.35	-0.359	14.52	-0.155	3.021

Table VI.

Simulation Data:

Range - 1000 Feet

Target RMS Acceleration - 3.5 G

Type A/C	Pilot Number	Elevator (δ) (Degrees)		Pitch Rate (q) (Degrees/Sec)		Lead Angle (λ) (Degrees)		LOS ($\dot{\lambda}_{T_A}$) (Degrees)		Error (ε) (Degrees)	
		Mean	RMS	Mean	RMS	Mean	RMS	Mean	RMS	Mean	RMS
F-4E	1	+0.059	2.129	-0.221	7.918	-0.080	2.826	-0.463	2.768	+0.336	2.186
	2	+0.000	2.151	-0.023	8.198	+0.004	2.893	-0.413	2.793	+0.412	2.251
	3	+0.073	2.128	-0.227	7.952	-0.082	2.878	-0.288	2.635	+0.208	1.971
F-5	1	+0.045	1.358	-0.285	7.693	-0.110	2.975	-0.114	2.439	+0.006	1.956
	2	+0.057	1.244	-0.357	7.334	-0.135	3.076	-0.403	3.096	+0.268	2.024
	3	+0.030	1.338	-0.190	7.358	-0.067	2.966	-0.739	2.092	+0.412	2.198
A-7	1	+0.040	4.929	-0.059	11.17	-0.021	3.917	-0.225	4.157	+0.205	2.721
	2	+0.462	4.938	-0.997	11.73	-0.343	3.918	-0.478	4.009	+0.137	2.676
	3	-0.117	4.893	+0.259	10.83	+0.091	3.850	-0.180	3.760	+0.274	2.597

Table VII.

Simulation Data:

Range - 1000 Feet

Target RMS Acceleration - 5.0 G

Type A/C	Pilot Number	Elevator (δ) (Degrees)		Pitch Rate (q) (Degrees/Sec)		Lead Angle (λ) (Degrees)		LOS (Σ_{T_A}) (Degrees)		Error (ϵ) (Degrees)	
		Mean	RMS	Mean	RMS	Mean	RMS	Mean	RMS	Mean	RMS
F-4E	1	+0.072	2.984	-0.277	11.15	-0.097	3.953	-0.224	3.801	+0.128	2.680
	2	-0.297	2.987	+0.286	11.41	+0.385	3.999	+0.316	3.647	-0.023	2.888
	3	+0.121	2.970	-0.384	11.05	-0.142	3.958	-0.399	3.604	+0.258	2.668
F-5	1	-0.036	1.849	+0.198	11.39	+0.089	4.323	+0.129	3.338	-0.039	3.305
	2	-0.227	1.783	+0.635	10.72	+0.270	4.346	-0.134	4.237	+0.403	2.876
	3	-0.046	1.707	+0.272	9.973	+0.111	4.240	+0.183	4.120	+0.082	2.327
A-7	1	+0.250	6.885	-0.471	15.47	-0.172	5.419	-0.377	5.706	+0.210	3.414
	2	+0.043	6.939	-0.132	16.45	-0.040	5.504	+0.128	5.757	-0.167	3.738
	3	-0.384	7.509	+0.679	14.84	+0.256	5.471	-0.107	4.820	+0.364	3.406

Appendix C

Pilot Data And "Pireps"*

The three pilots that "flew" the simulation were chosen for their flying experience in fighter-type aircraft. Table VIII summarizes that experience. All three are presently pursuing master of science degrees in engineering at the Air Force Institute of Technology and are thus well qualified to comment on the realism and authenticity of the simulation.

Given the fact that only longitudinal dynamics were simulated, the pilots generally thought that the simulation quite adequately represented vehicle and sight dynamics. In fact, it was suggested that maybe this simulator would by an inexpensive means of familiarizing new fighter pilots with the peculiarities of LCOS dynamics, and how to handle them.

Principal among the complaints concerning the simulation was the fact that extensive negative "G's" were necessarily required to track the zero-mean target motion. This just does not happen in reality. However, after a period of training, the pilots became used to pushing on the stick and their performance was not affected. The fact that there was no way to feel the aircraft "G" loading in the fixed-base simulator was also deemed detrimental,

*The term "pirep" comes from the weather forecasting terminology for pilot reports on weather conditions encountered aloft.

Table VIII.

Summary of Pilot Experience

Pilot (Total Flying Time)	Type Aircraft	Number Hours This Aircraft	Years Flown
Pilot #1 (2250 Hours)	T-37	125	1963 - 1964
	T-33	325	1965 & 1971 - 1972
	F-4C & D	1800	1965 - 1970
Pilot #2 (2100 Hours)	T-37/T-38	290	1966 - 1967
	F-102	65	1967
	F-101	420	1967 - 1969
	T-33	380	1967 - 1969
	F-4	400	1969 - 1970
	Hawker Hunter	25	1970
	B.A.C. Lightning	520	1971 - 1973
Pilot #3 (1959 Hours)	T-37/T-38	235	1966 - 1967
	F-100	680	1967 - 1969
	F-4	1044	1970 - 1973

but not greatly important.

Finally, the display on the oscilloscope did not allow the pilot the ability to see his "angle-off" the target--that angle formed by the extension of the longitudinal axes of the two aircraft. Again, the degrading effect was not deemed important.

In summary, they felt the simulation dynamics were quite authentic, however the negative "G" tracking and the primitive display tended to detract from the realism intended. It should be noted that this fact did not dampen their desire to do their very best in the performance of the task presented them.

Vita: Thomas R. Harvey

Thomas R. Harvey was born an Army "brat" [redacted] nown today as Vandenberg Air Force Base. After years of wandering from fort to fort, his family finally settled in Gainesville, Florida. Graduation from [redacted] was followed by four years at the Virginia Military Institute, from which he graduated in 1966 with a Bachelor of Science degree in Electrical Engineering, a commission as a Second Lieutenant in the United States Air Force, and a ticket to flight school. In 1968, after successfully completing Undergraduate Pilot Training at Laredo Air Force Base, Texas, he upgraded to the F-100 aircraft and subsequently spent a 14-month tour at Wheelus Air Base, Libya. There he was a range safety officer on the USAFE air-to-air and air-to-ground gunnery ranges, while maintaining his own proficiency in the F-100C and U-6A aircraft. Upon his return to the United States in 1970, he was assigned to fly C-141A aircraft out of Dover Air Force Base, Delaware. Two and a half years of flying global airlift ensued during which time he attained the position of aircraft commander. In 1972, he was selected for admission to the Air Force Institute of Technology, which he entered in August of that year. He graduated with the Master of Science degree in Astronautical Engineering, specializing in Guidance and Control, in March, 1974.

This thesis was typed [redacted]

PII Redacted

PII Redacted